Title

Precision Study of Supersymmetry at Future Linear {italic e}{sup +}{italic e}{sup -} Colliders

Authors

Tsukamoto, T.
Fujii, K.
Murayama, H.
et al.

Publication Date

1993-11-01

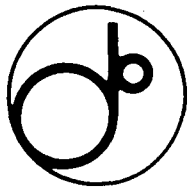

KEK Preprint 93-146
KEK-TH 374
LBL-34796
TU-449
November 1993
H

Precision Study of Supersymmetry at Future Linear e^+e^- Colliders*

Toshifumi Tsukamoto,[1] Keisuke Fujii,[1]
Hitoshi Murayama,[2,3] Masahiro Yamaguchi,[3] and Yasuhiro Okada[1]

[1] *National Laboratory for High Energy Physics (KEK)*
Tsukuba, 305 Japan
[2] *Theoretical Physics Group, Lawrence Berkeley Laboratory*
University of California, Berkeley, California 94720
[3] *Department of Physics, Tohoku University*
Sendai, 980 Japan

Abstract

We discuss a possible strategy for supersymmetry searches and studies at future linear e^+e^- colliders. We demonstrate their effectiveness by Monte Carlo analyses with full angular correlations under realistic experimental conditions including the initial state radiation and the beamstrahlung effects. The importance of precision measurements of supersymmetry parameters is emphasized. A detailed study on the first superparticle alone gives us an upper bound on the next superparticle. We can also test the basic mass relations assumed in grand unified models or supergravity, such as the gaugino mass relations or the universal scalar mass assumption in a variety of ways. The polarized electron beam plays a crucial role in this study.

*This work was supported in part by the Director, Office of Energy Research, Office of High Energy and Nuclear Physics, Division of High Energy Physics of the U.S. Department of Energy under Contract DE-AC03-76SF00098.

National Laboratory for High Energy Physics, 1993

KEK Reports are available from:

Technical Information & Library
National Laboratory for High Energy Physics
1-1 Oho, Tsukuba-shi
Ibaraki-ken, 305
JAPAN

Phone: 0298-64-1171
Telex: 3652-534 (Domestic)
(0)3652-534 (International)
Fax: 0298-64-4604
Cable: KEK OHO
E-mail: LIBRARY@JPNKEKVX (Bitnet Address)
library@kekvax.kek.jp (Internet Address)

DISCLAIMER

1 Introduction

The e^+e^- colliders have been playing complementary roles to the hadron colliders in high energy experiments. In general, e^+e^- colliders have reasonable signal rates in a clean environment with a definite center-of-mass energy, enabling us to perform precision measurements of particle masses, lifetimes, and various differential cross sections, while hadron colliders provide opportunities to quickly survey high energy frontier. In spite of various beam-beam effects[1] including mini-jet productions[2], this cleanness persists up to TeV region[3, 4]. In addition, future linear e^+e^- colliders such as JLC [5, 4] will be equipped with a highly polarized beam using strained Gallium Ascenide or superlattice [6, 7], with which a beam polarization of $P_{e^-} > 90$ % is expected.

SLC and LEP experiments demonstrated fully the above virtues of e^+e^- colliders. The precision measurements on the Z^0 resonance are now sensitive to one-loop quantum corrections, and have put a stringent constraint on the top quark mass [8]. Furthermore, the measured Weinberg angle $\sin^2\theta_W$ turned out to exclude the minimal model of the grand unified theory (GUT), but is consistent with its supersymmetric (SUSY) version. This observation raised revived interests in the SUSY models. SUSY predicts many new particles below TeV region. An e^+e^- collider is an ideal device to search for colorless superparticles which are believed to be relatively light compared to colored ones.

The aim of the present paper is to demonstrate the effectiveness of future linear e^+e^- colliders in the study of the colorless superparticles. We focus not only on their discoveries, but also on the precise determinations of supersymmetry parameters. The importance of the precision measurements of the parameters is two-fold. (1) Once we discover at least one superparticle, we can measure its properties and extract information on the SUSY parameters which puts upper bounds on the next superparticles. We can thus set the next target center-of-mass energy to go up to. This property of the supersymmetric models permits us to successively find new particles one after another. (2) The supersymmetric grand unification models (GUT) or the minimal supergravity scenario predict certain relations among the superparticle masses. We can test these relations and verify or exclude such models. For these purposes, the polarized electron beam plays an essential role.

The analyses presented in this paper are guided by the following working hypothesis. Our input parameters are taken within the minimal supergravity scenario, but we reproduce them after Monte Carlo simulations with realistic detector and machine parameters including the initial state radiation and the beamstrahlung effects, and demonstrate that the mass relations in the scenario can be tested experimentally. We focus on the strategy, not on the search limits, of the experiments at future linear e^+e^- colliders.

We first take a definite parameter set in the minimal supergravity scenario, assuming the universal scalar mass and GUT-relation of the gaugino masses. Then we start with the lightest detectable superparticle ("first superparticle") which is a right-handed slepton in our choice of the SUSY parameters. By analyzing its properties in detail, we draw an upper bound on the next superparticle (chargino and second neutralino) using the GUT-relation of the gaugino masses, and simultaneously test the universal scalar mass assumption between the first and the second generations. Raising the center-of-mass energy to the next expected threshold, we study the chargino and again obtain a useful upper bound on the next to the next superparticle (left-handed slepton) by extracting the t-channel sneutrino contribution. Its precise study again allows a stringent test on a consequence of GUT (the GUT-relation of the gaugino masses). In this way, we can successively find many superparticles from the lightest to heavier ones, and also can make crucial tests on the GUT or supergravity assumptions.

The paper is organized as follows. In Section 2, we take a typical parameter set for which the "first superparticle" is a right-handed slepton. We perform Monte Carlo analyses along the line just described. In Section 3, we examine another case with a different parameter set, where the chargino is the "first superparticle". We also discuss possible difficulties we may encounter in the study of superparticles. Section 4 concludes this paper. Appendix A summarizes the important mass relations within the GUT or supergravity models which are relevant to the analyses in this paper. A brief description of our Monte Carlo simulator is given in Appendix B, where the methods to incorporate the interference and angular correlations are also explained.

2 Strategy in a Light Slepton Case

In this section, we describe superparticle searches at a future linear e^+e^- collider for a sample case, where the right-handed slepton is the "first superparticle". We emphasize the importance of precision measurements of masses, total and differential cross sections; one can extract useful information on the next superparticle from such measurements. Moreover, we will be able to test various assumptions in SUSY-GUT or supergravity models.

The parameter set we take in our analyses is

$$\begin{aligned} m_0 &= 70 \text{ GeV}, \\ M_2 &= 250 \text{ GeV}, \\ \mu &= 400 \text{ GeV}, \\ \tan\beta &= 2, \end{aligned} \tag{1}$$

which gives the following light superparticle mass spectrum:

$$\begin{aligned} \tilde{\chi}_1^0 &: \ 117.8 \text{ GeV}, \\ \tilde{l}_R &: \ 141.9 \text{ GeV}, \\ \tilde{\chi}_1^\pm &: \ 219.3 \text{ GeV}, \\ \tilde{\chi}_2^0 &: \ 221.5 \text{ GeV}, \\ \tilde{\nu}_L &: \ 227.2 \text{ GeV}, \\ \tilde{l}_L^\pm &: \ 235.5 \text{ GeV}. \end{aligned} \tag{2}$$

Note that this parameter set also makes $\tilde{\chi}_1^0$ as a good candidate for cold dark matter.

2.1 Right-handed Slepton

The production of right-handed sleptons occurs via the Feynman diagrams shown in Fig.1. The three generations of the right-handed sleptons, $\tilde{e}_R$, $\tilde{\mu}_R$, and $\tilde{\tau}_R$, are usually assumed

to be mass-degenerate by the "universal scalar mass" assumption (see Appendix A). Among them, only the $\tilde{e}_R$-pair production process has the t-channel diagram of neutralino exchange. Note that only the bino ($\tilde{B}$) component appears in this diagram, though the neutralino mass-eigenstates may differ significantly from the pure bino state. $\tilde{\mu}_R$ and $\tilde{\tau}_R$ have only the s-channel γ- and Z^0-exchange diagrams, and the cross section and the angular distribution are determined solely by their gauge quantum numbers and spin. The production cross section of $\tilde{e}_R$ pairs is shown in Fig.2-a), which shows that the process has a relatively large cross section of $O(100)$ fb. The decay has a 100 % branching fraction into $e\tilde{\chi}_1^0$, since it is the only kinematically available channel allowed by the R-parity and the lepton number conservation, as long as the right-handed slepton is the "first superparticle". Therefore, the event signature to look for is an acoplanar lepton pair with large missing energy.

We generated signal and background events for the right-handed sleptons at $\sqrt{s} = 350$ GeV. The event generation includes the effect of the initial state radiation as well as the beamstrahlung effects (for details, see the appendix B). The events with such a signature were selected from the generated events by the following criteria:

1. e^+e^- or $\mu^+\mu^-$ with 5 GeV $< E_l < (\sqrt{s} - 100$ GeV$)/2$,
2. 20 GeV $< E_{vis} < \sqrt{s} - 100$ GeV,
3. $|m_{ll} - m_Z| > 10$ GeV,
4. $|\cos\theta_{l^\pm}| < 0.9$,
5. $-Q \cdot \cos\theta_l < 0.75$ where Q is the charge of the lepton, and the polar angle is measured from the electron beam direction.

Cut 3 is to eliminate background events from the $e^+e^- \to Z^0Z^0$ process where one Z^0 decays into a charged lepton pair and the other into a neutrino pair. Cuts 4 and 5, on the other hand, reduce the background from the W^+W^- and $e^\pm \overset{(-)}{\nu}_e W^\mp$ productions. Fig.3-a) shows the acoplanarity distribution for the selected electron pairs from the $\tilde{e}_R$ decays (solid), together with the background from W^+W^- (dash) and $e^\pm \overset{(-)}{\nu}_e W^\mp$ (dot). There is a clear excess over the background in the distribution. For the $\tilde{\mu}_R$ pairs, the signal-to-background ratio is lower than the $\tilde{e}_R$ case (see Fig.3-b)) due to the lower cross section (see Fig.2-b)). One can, however, use a right-handed electron beam, which enhances the signal and, at the same time, suppresses the background dramatically, as shown in Fig.3-c)[9]. We assume a beam polarization of $P_{e^-} = 95$ % hereafter, and impose an additional cut on the acoplanarity angle:

6. $\theta_{acop} > 30°$.

The resultant detection efficiencies are 45.0 % for the $\tilde{e}_R$ pairs and 54.2 % for the $\tilde{\mu}_R$ pairs with essentially no background.

The first analysis which should be performed on this clean event sample is to extract the masses of the sleptons and $\tilde{\chi}_1^0$ from the decay energy distribution of the final-state

leptons. Thanks to the simple two-body kinematics, the distribution should be flat with its two edges determined by the slepton and the LSP masses. We show in Fig.4-a) the energy distribution of the final-state μ's for an integrated luminosity of 20 fb^{-1}. For the $\tilde{e}_R$ case, the measurement is easier since the cross section is higher. By making a two-parameter fit to the spectrum, we can determine their masses with a statistical error of ± 1 %, as shown in Fig.4-b).

It is also interesting to study the angular distribution of the sleptons. Once we know the slepton and the LSP masses, we can determine the slepton four-momenta from the final-state lepton momenta with a two-fold ambiguity. Fig.5-a) plots the two solutions for the reconstructed $\tilde{\mu}_R$'s. Fortunately, the "wrong" solutions have a flat angular distribution, which can be easily subtracted to obtain Fig.5-b). The figure clearly shows that the distribution behaves like $\sin^2\theta$, characteristic of the s-channel pair production of scalar particles. The similar distributions for the selected $\tilde{e}_R$'s are shown in Figs.6-a) and -b), where one can see a clear forward peak indicating the t-channel neutralino exchange. Since we already know the LSP mass, this distribution suggests that the LSP is dominated by the bino component. If the LSP is dominated by the higgsino component, the distribution should look like that of the $\tilde{\mu}_R$-pair production.

One can also measure the polarization dependence of the cross sections. For the $\tilde{e}_R$ pair production process, the t-channel $\tilde{B}$ exchange diagram contributes only to the production from the right-handed electron beam. If the beam is left-handed, therefore, only the s-channel diagrams exist. Note that if $\tilde{\chi}_1^0$ is almost a pure higgsino, then its t-channel contribution is highly suppressed, and we expect $\sigma_R \simeq 4\sigma_L$, where the factor of 4 is simply the squared ratio of the hypercharges of e_L and e_R. If $\tilde{\chi}_1^0$ is almost a pure bino, then its t-channel exchange dominates over the s-channel diagram, and the cross section σ_R is much larger than $4\sigma_L$. Thus the cross sections alone give important information on the neutralino sector. Combined with the angular distribution, we obtain useful constraints on the $(M_2, \mu, \tan\beta)$ space from the slepton analysis, though we will not go into the analysis here.

The most important information we can extract from the slepton pair production is an upper bound on the lighter chargino ($\tilde{\chi}_1^\pm$) mass. One obtains the upper bound from the $\tilde{\chi}_1^0$ mass by assuming the GUT-relation of the gaugino masses and the minimal particle content in the neutralino and chargino sectors. Fig.7-a) shows this upper bound. One can intuitively understand this bound as follows. If $\tilde{\chi}_1^0$ is almost a pure higgsino, then $\tilde{\chi}_1^\pm$ is also almost a pure higgsino, and they should be nearly mass-degenerate. If $\tilde{\chi}_1^0$ is almost a pure bino, then $\tilde{\chi}_1^\pm$ is almost a pure wino, which is $\frac{3}{5}\cot^2\theta_W = 2.0$ times as heavy as $\tilde{\chi}_1^0$. Since the reality is between these two extremes, $\tilde{\chi}_1^\pm$ should be lighter than $2.0 m_{\tilde{\chi}_1^0}$. A similar upper bound can be obtained for the second neutralino $\tilde{\chi}_2^0$ as well, as seen in Fig.7-b). Therefore, the next target energy we should go up to is that for the associated $\tilde{\chi}_2^0\tilde{\chi}_1^0$ production or that for the pair production of $\tilde{\chi}_1^\pm$ or $\tilde{\chi}_2^0$. If they are not discovered within the predicted mass range, then the GUT-relation is disproved, and SUSY-GUT, at least that with the minimal particle content, faces a severe difficulty [10]. The upper bounds in our sample case are

$$m_{\tilde{\chi}_1^\pm}, m_{\tilde{\chi}_2^0} < 2.0 m_{\tilde{\chi}_1^0} \simeq 240 \text{ GeV}. \tag{3}$$

The slepton mass determinations are in themselves very important, since they allow us an essential test on the minimal supergravity scenario, whether the scalar masses are generation-independent or not. Fig.8 shows the test on the generation independence of the measured masses of $\tilde{e}_R$ and $\tilde{\mu}_R$.

Tables 1 and 2 summarize the observable quantities for the right-handed slepton production and their implications, respectively.

2.2 Neutralino Associated Production

Since we now have the upper bound on the mass of $\tilde{\chi}_2^0$, we can set the energy to study the $\tilde{\chi}_1^0\tilde{\chi}_2^0$ associate production process at $\sqrt{s} = 400$ GeV. Unfortunately the cross section for this process is rather low, $O(10)$ fb for our parameter set, and there is the large "background" from the right-handed slepton pair production, though the background from the W-pair production can be effectively suppressed by using the right-handed electron beam at the cost of some loss of the signal cross section [11]. Therefore, this process can be used only to check the existence of $\tilde{\chi}_2^0$ predicted from the LSP mass and the GUT-relation.

In our parameter choice, the dominant decay mode is $\tilde{\chi}_2^0 \to \tilde{l}_R^{\pm} l^{\mp}$ and its charge conjugate, which leads to a final state consisting of an acoplanar lepton pair with large missing energy. Such events can be selected with the same criteria as with the right-handed slepton pair. Fig.9-a) is the scatter plot of the muon energies for an integrated luminosity of 20 fb^{-1} and a beam polarization of $P_{e^-} = 95\%$. The background from the W^+W^- production is very small thanks to the beam polarization (see Fig.9-b)). The "background" from the right-handed slepton pair has much lower lepton energies as shown in Fig.9-c), while that from the $\tilde{\chi}_2^0$ decay has higher energies. Therefore, one can verify the existence of $\tilde{\chi}_2^0$, though the statistics is too low for its precise studies. The $\tilde{\chi}_2^0$ mass can be measured, however, using its pair production: though the $\tilde{\chi}_2^0$ mass is similar to that of $\tilde{\chi}_1^{\pm}$ for our parameter set, we can easily separate $\tilde{\chi}_2^0$-pair events from $\tilde{\chi}_1^{\pm}$-pair events by using the four-lepton final state from a $\tilde{\chi}_2^0$ pair which is essentially background-free.

2.3 Chargino Pair Production

Considering the upper bound on the mass of the lighter chargino from the right-handed slepton studies, we fix the center-of-mass energy at $\sqrt{s} = 500$ GeV. If we do not discover the chargino below the upper bound, then it will disprove SUSY-GUT, at least that with the minimal particle content [10]. If we discover it, then we can measure the parameters of the neutralino/chargino sector precisely. What is most exciting here is that we can test whether the GUT-relation on the gaugino masses holds or not.

For the parameters in our sample case, the chargino decays mainly into a two-body final state: $\tilde{\chi}_1^{\pm} \to \tilde{\chi}_1^0 W^{\pm}$. The event signature is thus an acoplanar W pair with large missing energy. The W bosons in the final state can be easily reconstructed by the jet invariant mass method[12]. We use the following selection criteria to select such events in the four-jet mode:

1. the number of charged tracks > 20,

2. 20 GeV $< E_{vis} < \sqrt{s} - 100$ GeV,
3. there is no lepton (e or μ) with $E_l > 25$ GeV,
4. there exists a y_{cut} greater than 5×10^{-3} resulting in four jets, two of which satisfy $|\cos\theta_j| < 0.8$ and the remaining two satisfy $|\cos\theta_j| < 0.95$.
5. the four jets can be grouped into two pairs of jets consistent with the W mass, $m_W - 10$ GeV $< m_{jj} < m_W + 20$ GeV,
6. each of the two W candidates has a production angle $|\cos\theta_W| < 0.9$,
7. the missing mass is inconsistent with the $W^+W^-Z^0(\to \nu\bar{\nu})$ hypothesis, $m_{missing} \leq 70$ GeV or $m_{missing} \geq 120$ GeV, and
8. $\theta_{acop} > 30°$.

The detection efficiency after these cuts was estimated to be 10.8 %, including the branching fraction into the four-jet final states. Fig.10 shows the acoplanarity angle distribution for the remaining events after all but the acoplanarity cut, when an integrated luminosity of 50 fb^{-1} is accumulated. One can clearly see an excess over the background from the W^+W^- (dash), the $e^+e^-W^+W^-$ (dot), and the sum of the $e^{\pm}\overset{(-)}{\nu_e}W^{\mp}Z^0$, $W^+W^-Z^0$, and $\nu_e\bar{\nu}_e W^+W^-$ (dot-dash) productions. The selection cuts effectively remove, to a negligible level, the background from the other processes such as $e^+e^- \to Z^0Z^0$, $Z^0Z^0Z^0$, and $\nu_e\bar{\nu}_e Z^0Z^0$. The distribution of the W energies is flat thanks to the simple two-body kinematics. Monte-Carlo data including the detector and the beam effects suggest this simple kinematics as shown in Fig.11-a). A fit to the event sample gives the masses of $\tilde{\chi}_1^{\pm}$ and $\tilde{\chi}_1^0$ (see Fig.11-b)). Here we can make a cross-check on the mass of $\tilde{\chi}_1^0$ by comparing it with that measured for the slepton production. For an integrated luminosity of 50 fb^{-1}, the error on the $\tilde{\chi}_1^{\pm}$ mass is expected to be ± 10 GeV. This error reduces to ± 5 GeV when combined with the $m_{\tilde{\chi}_1^0}$ measured for the right-handed slepton decays.

One can also study the angular distribution of $\tilde{\chi}_1^{\pm}$'s. Similarly to the case in the right-handed slepton-pair production, one can determine the four-momenta of the charginos up to a two-fold ambiguity, once their masses are known. Fig.12-a) plots the angular distribution with the two-fold ambiguity unresolved. The "wrong" solutions again give an almost flat distribution, which can be subtracted to reproduce the real angular distribution as shown in Fig.12-b)[13]. The event excess in the forward region suggests that there is some diagram with t-channel particle exchange. The only particle exchanged in the t-channel here is the electron sneutrino $\tilde{\nu}_{e_L}$.

An important analysis can be made with the beam polarization. Recall that the charged wino $\tilde{W}^{\pm}$ is not produced from the right-handed beam just like the W boson (suppressed by a factor of $(m_Z^2/s)^2 < 10^{-3}$ in our case), while the charged higgsino $\tilde{H}^{\pm}$ has roughly the same cross sections (up to a factor of ~ 4) for the left- and the right-handed electron beams. Thus the cross section for the right-handed electron beam "measures" the

higgsino component of the chargino. We have four independent observables concerning the neutralino/chargino sector:

$$m_{\tilde{\chi}_1^0},\ m_{\tilde{\chi}_1^\pm},\ \sigma_R(\tilde{e}_R),\ \sigma_R(\tilde{\chi}_1^\pm). \tag{4}$$

The masses are directly related to the neutralino/chargino mass matrix. The cross section $\sigma_R(\tilde{e}_R)$ has the contribution from the t-channel neutralino exchange. $\sigma_R(\tilde{\chi}_1^\pm)$ carries the information on the higgsino component in $\tilde{\chi}_1^\pm$. Then we can perform a global fit, varying the following parameters:

$$M_1,\ M_2,\ \mu,\ \tan\beta, \tag{5}$$

from which we can test the GUT-relation $M_1/M_2 = \frac{5}{3}\tan^2\theta_W$. Fig.13 shows the resultant $\Delta\chi^2 = 1$ contour in the M_1 and M_2 plane. In this way, we can test the SUSY-GUT prediction at the $O(5)$ % level[14].

Another important information can be obtained from the cross section for the left-handed electron beam, which was not used in the fit. The left-handed electron beam allows a t-channel exchange of $\tilde{\nu}_e$, which interferes destructively with the s-channel gauge boson exchange diagrams. Since we already know the composition of the chargino from the previous analysis, the only unknown parameter here is the mass of $\tilde{\nu}_e$. We show in Fig.14 the dependence of the cross section on $m_{\tilde{\nu}_e}$ for $P_{e^-} = 0$. In our choice of parameters, the cross section is near the minimum, and we can measure the mass of $\tilde{\nu}_e$ fairly well. The measured $\tilde{\nu}_e$ mass sets an upper bound on the mass of the left-handed slepton $\tilde{e}_L$ (see Appendix A)[15]:

$$m_{\tilde{e}_L}^2 \leq m_{\tilde{\nu}_e}^2 + 0.77 m_Z^2. \tag{6}$$

Thus we have again the next target energy to hunt the next superparticle.

Tables 3 and 4 summarize the observables and their implications for the chargino production, respectively.

2.4 Left-handed Slepton

The production of the left-handed slepton occurs first in the associate production process, $e^+e^- \to \tilde{e}_L^\pm \tilde{e}_R^\mp$. The Feynman diagram is shown in Fig.15. Here, only the t-channel $\tilde{B}$-exchange contributes, and s-channel gauge boson exchange diagrams are absent due to the "chirality" of the scalar particles in the supersymmetric gauge theory. The cross section is reasonable if $\tilde{B}$ is relatively light. Since we already know that the chargino/neutralino parameters by this moment, we can make definite prediction of the cross section and angular distribution with the only one unknown parameter, $m_{\tilde{e}_L}$.

Fig.2-a) shows the cross section for $e^+e^- \to \tilde{e}_L^\pm \tilde{e}_R^\mp$. Notice that the cross section increases as β in the threshold region, contrary to that of the $\tilde{l}_R$- or $\tilde{l}_L$-pair production which rises as β^3. This is due to the S-wave production of the sleptons which demonstrates the conservation of chirality that left(right)-handed selectrons couple only to left(right)-handed electrons. Since this chiral selection rule is essential to ensuring the absence of quadratic divergences in scalar masses in supersymmetric theories, its experimental test is interesting.

The decay of the left-handed slepton may be a little complicated. Fig.16 gives the branching fractions into the two-body final state $\tilde{e}_L \to e\tilde{\chi}_1^0$ for various parameters. As the scalar mass becomes heavier, the left-handed slepton tends to decay into multi-body final states. Nevertheless, there is still more than $O(10)$ % branching fractions into the two-body final state. For our parameter set, the two-body decay mode is actually dominant.

We set the center-of-mass energy at $\sqrt{s} = 400$ GeV[16] and employ the same selection criteria used for the right-handed slepton-pair production, which result in an overall detection efficiency of 44.5 %. Here again, the W-pair production, which would be the largest background, can be effectively suppressed by the use of the right-handed electron beam, leaving the $\tilde{e}_R$-pair production as the dominant background. Notice, however, that the charge of the produced selectrons is uniquely fixed for a 100 %-polarized beam: $e^+e_R^- \to \tilde{e}_L^+\tilde{e}_R^-$. Fig.17 is the scatter plot of the electron and positron energies for an integrated luminosity of 20 fb^{-1} and a realistic polarization $P_{e^-} = 95$ %. The figure shows that the events from the $\tilde{e}_R$-pair and the associate productions are clearly separated[17]. We perform a two-parameter fit to the energy distribution of the positrons to determine the left-handed slepton mass (see Figs.18-a) and -b)). The expected error on the $\tilde{e}_L$ mass is ± 2.5 GeV for an integrated luminosity of 20 fb^{-1}. A consistency check between the measured $m_{\tilde{\chi}_1^0}$ with those measured for the $\tilde{l}_R$- and $\tilde{\chi}_1^\pm$-pair productions can be made, and the sensitivity to $m_{\tilde{e}_L}$ can be further improved by including in the fit the $m_{\tilde{\chi}_1^0}$'s measured earlier.

The comparison of the masses of $\tilde{e}_R$ and $\tilde{e}_L$ is of our great interest. The difference $m_{\tilde{e}_L}^2 - m_{\tilde{e}_R}^2$ directly reflects the mass difference of the $\mathbf{5}^*$ and the $\mathbf{10}$ representations of the $SU(5)$-GUT, while the universal scalar mass assumption in the minimal supergravity predicts that they are the same. Fig.19 compares the so determined values with the prediction.

After measuring the $\tilde{e}_L$ mass, the generation universality assumed in the supergravity scenario tells us that $\tilde{\mu}_L$ and $\tilde{\tau}_L$ are mass-degenerate with $\tilde{e}_L$. Then we can go up to the threshold of their pair productions.

Tables 5 and 6 summarize the observables and their implications for the slepton associate production, respectively.

2.5 Heavier Superparticles

Instead of presenting detailed analyses on the heavier superparticles, whose masses are presumably predicted by this point of the SUSY studies, we briefly discuss some features of their searches below.

The $\tilde{\chi}_2^0$-pair production has a very clean signal of acoplanar four-leptons, which is essentially background-free. The $\tilde{l}_L$-pair production has a higher rate for the left-handed electron beam, but it is probably better to employ the right-handed electron beam in order to avoid the W-pair background. The $\tilde{e}_L$-pair production has t-channel exchange diagrams of both $\tilde{B}$ and $\tilde{W}$ components of neutralinos, and its cross section and angular distribution is worth studying.

After studying the right-handed sleptons, the lighter chargino, the second neutralino, and the left-handed sleptons, we will probably reach the thresholds of other heavy su-

perparticles as well, like the heavier chargino, and the heavier neutralinos which may decay into charged particles. After crossing these thresholds, the experiment becomes quite messy. We know, however, the basic parameters of the chargino/neutralino sector already, and we can still make a consistency check of the measured parameters, comparing the observed events with the Monte-Carlo predictions. The resulting events are highly dependent on the precise values of the parameters, and we believe it is premature to perform a Monte-Carlo analysis in this paper.

The most important physics goal above the thresholds of the heavier superparticles is to test the overall consistency of the events with the supersymmetric Lagrangian. Since the supersymmetric Lagrangian is tightly constrained, the overall consistency is a measure whether the interactions are indeed described by a supersymmetric theory or not [18].

3 Discussions on Other Cases

In the previous section, we have extensively studied the SUSY search and study strategy for a particular choice of SUSY parameters, where we demonstrated how the precise studies, possible only at an e^+e^- collider, give useful information on the next superparticles, with which we can go up to higher energies, step by step, with some confidence. In this section, we discuss how the situation changes, when we take different sets of parameters.

3.1 Chargino Lighter than Slepton

It is also possible that the chargino is lighter than the right-handed sleptons. In this case, we will discover the chargino first.

The Feynman diagrams for the chargino-pair production are shown in Fig.20. Note that there is a t-channel exchange diagram of electron-sneutrino $\tilde{\nu}_e$, which contributes to the process only if the electron beam is left-handed. The cross section for the right-handed electron beam is determined solely by the chargino parameters.

In a large fraction of the chargino parameter space (M_2, μ), the lightest chargino decays into the two-body final state: $\tilde{\chi}_1^\pm \to \tilde{\chi}_1^0 W^\pm$. Since the daughter W's can be easily reconstructed by the jet invariant mass method, we can study the acoplanarity distribution of the final-state W's, as we did in the previous section. If the chargino decays into a three-body final state, however, the situation will be somewhat more complicated. Nevertheless, we can still do a good job as long as the chargino decay has a sufficient Q-value.

As a case very different from the example given in the previous section, we study a chargino with a large higgsino component in this section. The parameters we choose here are

$$\begin{aligned} m_0 &= 400 \text{ GeV}, \\ \mu &= 250 \text{ GeV}, \\ M_2 &= 400 \text{ GeV}, \\ \tan\beta &= 2, \end{aligned} \tag{7}$$

which give

$$\begin{aligned} \tilde{l}_R &: \ 444.1 \text{ GeV}, \\ \tilde{\chi}_1^\pm &: \ 219.3 \text{ GeV}, \\ \tilde{\chi}_1^0 &: \ 169.2 \text{ GeV}. \end{aligned} \tag{8}$$

In such a higgsino-dominant case, the mass difference between the lighter chargino and the LSP is in general small ($\Delta m \simeq 50$ GeV $< m_W$ here), and the chargino decays mainly into a three-body final state to which the analysis in the previous section does not apply at all.

We describe here our chargino selection at $\sqrt{s} = 500$ GeV in the higgsino-dominant case. Although the best way to search for the higgsino-dominant chargino is again to use the four-jet final state, we consider the lepton+two-jet mode for mass measurements: it is hard to select a jet pair resulting from a single chargino decay out of the four jets, since the jet pair now does not have any fixed invariant mass. Our selection criteria are

1. the number of tracks ≥ 5 which includes an energetic isolated e or μ ($E_l > 5$ GeV and the energy deposited by the other particles within the cone of a half-angle 30° around the lepton track is < 1 GeV),
2. 20 GeV $< E_{vis} < \sqrt{s} - 100$ GeV,
3. there are two jets for some $y_{cut} > 5 \times 10^{-3}$ with $m_{jj} < m_W - 12$ GeV and $E_{jj} < (\sqrt{s} - 100 \text{ GeV})/2$,
4. $|\cos\theta_j| < 0.9$, $|\cos\theta_l| < 0.9$, $-Q \cdot \cos\theta_l < 0.75$, $-Q \cdot \cos\theta_{jj} < 0.75$, where Q is the lepton charge and θ_{jj} is the polar angle of the total momentum of the two-jet system,
5. $|m_{l\nu} - m_W| > 10$ GeV for the W-pair hypothesis.

Cuts 3 to 5 are to reduce the background from the W-pair and the $e^\pm \overset{(-)}{\nu}_e W^\mp$ productions[19]. Fig.21 plots the acoplanarity angle between the lepton momentum and the total momentum of the two jets for the signal events (solid) and the background events from $e^+e^- \to W^+W^-$ (dash) and $e^\pm \overset{(-)}{\nu}_e W^\mp$ (dot), where an integrated luminosity of 20 fb^{-1} is assumed. It is clear from the figure that, when we apply an acoplanarity cut:

6. $\theta_{acop} > 30°$,

we can obtain a fairly pure event sample of the charginos. After this final cut, the detection efficiency is 10.3 % and we obtain the total energy distribution of the two jets in Fig.22-a), which gives us the mass of the chargino. A two-parameter fit to the distribution, varying the chargino and the LSP masses yields the contours shown in Fig.22-b). We can determine their masses with statistical accuracies of ± 2.0 GeV and ± 1.5 GeV, respectively, given an integrated luminosity of 20 fb^{-1}.

Once the masses and cross sections are measured, one can perform similar analyses as in the previous section. One can determine ($M_2, \mu, \tan\beta$) from the chargino mass, the LSP mass, and the total cross section from the right-handed electron beam, assuming the

GUT-relation of the gaugino masses[20]. Then we can predict the masses of the second neutralino, the second chargino, *etc*, and can set the energy for the next threshold. If we do not discover them at the predicted masses, the SUSY-GUT with the minimal particle content is excluded. The angular distribution and the cross section for the left-handed electron beam give us the sneutrino mass, from which we obtain an upper bound on the left-handed slepton mass without any assumptions. By further assuming the universal scalar mass at the GUT-scale $m_{\mathbf{5}^*} = m_{\mathbf{10}}$, we can also obtain an upper bound on the right-handed slepton mass. Then we can set the next target energy at the threshold of the right-handed slepton pair production. If we do not discover the right-handed slepton within the predicted mass range, the universal scalar mass assumption is violated (at least within the minimal particle content).

In this way, a systematic study on SUSY particles can be done for the lighter chargino case just as in the lighter slepton case.

3.2 Complications

A complication occurs when several species of superparticles have nearly degenerate masses. Their thresholds open almost simultaneously, and it is in general hard to tell which event comes from which reaction. For example, some of the charginos and the neutralinos may be nearly mass-degenerate and their signals overlap with each other. Even in such a case, energy scan, possible only at an e^+e^- collider, helps us sort out the signals: once some signals of new particles are found, we can carry out an energy scan in small steps to determine their thresholds. Another advantage of the e^+e^- collider is that any decay modes can be used to select the signal, while only those including some energetic lepton are useful at hadron colliders. One of such examples is already demonstrated in Section 2. In our choice of parameters in Section 2, we have both the $\tilde{\chi}_1^0\tilde{\chi}_2^0$ associate production and the $\tilde{e}_L\tilde{e}_R$ associate production at $\sqrt{s} = 400$ GeV. We could, however, resolve them, since $\tilde{e}_L$ decays only into an electron but $\tilde{\chi}_2^0$ has the muon mode as well. The thresholds for the $\tilde{\chi}_1^\pm$- and the $\tilde{\chi}_2^0$-pair productions were also close to each other. There, we have used the hadronic final state from $\tilde{\chi}_1^\pm \to \tilde{\chi}_1^0 W^\pm$, which is absent for $\tilde{\chi}_2^0$: $\tilde{\chi}_2^0$ only decays leptonically.

Heavier superparticles generally undergo cascade decays, which complicate the analyses. We emphasize again that e^+e^- colliders can gradually raise the center-of-mass energy so that the lightest one is discovered first, and its analysis is very simple as we demonstrated in the previous sections. By studying the first several superparticles precisely, we can determine at least some of the supersymmetry parameters. The complicated cascade decays occur probably only for the heavier superparticles. Therefore, we have enough time before facing the complication due to the cascade decay.

3.3 Highly Degenerate Spectrum

When the decay of a superparticle has a very low Q-value, its detection becomes very difficult. A typical example is the higgsino-dominant chargino when $\mu \ll M_2$: the first chargino, $\tilde{\chi}_1^\pm$, is nearly mass-degenerate with the first and the second neutralinos, $\tilde{\chi}_1^0$ and $\tilde{\chi}_2^0$. The β-decay of $\tilde{\chi}_1^\pm$ with a low Q-value,

$$\tilde{\chi}_1^+ \to \tilde{\chi}_1^0 \nu_l l^+,\ \tilde{\chi}_1^0 q\bar{q}, \tag{9}$$

is hard to detect, even if its production cross section is large. The minimal detectable mass difference $\Delta m = m_{\tilde{\chi}_1^\pm} - m_{\tilde{\chi}_1^0}$ had been estimated to be 20 GeV in [21]. We believe that this limitation can be relaxed considerably by using the right-handed electron beam which kills most of the major background such as $e^+e^- \to W^+W^-$, $e^\pm \overset{(-)}{\nu}_e W^\mp$, *etc*, while keeping a reasonable signal cross section. A dedicated study is necessary for this case, since the higgsino-dominant neutralino/chargino may be the "first superparticle."

4 Conclusion

We have carried out detailed Monte Carlo simulations of SUSY productions at a future linear e^+e^- collider for a typical choice of SUSY parameters. The simulations took into account realistic experimental conditions imposed by the machine and the detector thereat. The results of the simulations demonstrated the effectiveness of the e^+e^- collider which can be summarized as follows.

The e^+e^- machine provides not only an efficient way to discover supersymmetric particles but also a unique possibility of precision studies such as mass determinations and differential cross section measurements. It should be emphasized that this virtue of the e^+e^- collider crucially depends on its cleanness, well defined initial state, and the availability of a highly polarized electron beam. In particular, the polarized electron beam will be an essential tool to control background and to sort out various components of a mass-eigenstate. We have found that, from the first superparticle alone, we can learn a lot about the supersymmetry parameters, which guide us to the discovery of the next. This process will repeat itself until we exhaust all the superparticles kinematically accessible. More importantly, the parameter determinations through the measurements of the superparticle masses and cross sections enable us to test some key assumptions in supersymmetric grand unified models or supergravity, such as the gaugino mass relations and the universal scalar mass.

ACKNOWLEDGMENT

The authors wish to thank the members of the Japan Linear Collider physics working group for valuable discussions and suggestions. Among them, K. Hikasa and S. Orito deserve special mention: K. Hikasa's "JLC SUSY Manual" benefited the authors greatly in the development of the SUSY event generators and S. Orito's continuous encouragement was essential to the completion of this work. The authors are also grateful to T. Kon and M. Jimbo for helping us check out the cross section formulas with beam polarization and to J. Kanzaki, Y. Kurihara, and A. Miyamoto for letting us use their background event generators.

This work was supported in part by the Director, Office of Energy Research, Office of High Energy and Nuclear Physics, Division of High Energy Physics of the U.S. Department

of Energy under Contract DE-AC03-76SF00098.

A Brief Review of Superparticle Mass Spectrum

In this appendix, we briefly review properties of the minimal supersymmetric standard model (MSSM) used in this paper and discuss mass relations among superparticles.

We assume the minimal particle content of the supersymmetric standard model. We also assume that the lightest superparticle (LSP) is stable due to the R-parity conservation, or at least its life-time is long enough so that it does not decay in a detector. Then signals of superparticles are associated with missing energies.

The superparticles are classified into the following sectors: neutralinos, charginos, sleptons, squarks, and gluinos. The neutralino sector in the MSSM consists of the two neutral gauginos, $\tilde{B}$ (bino), $\tilde{W}^3$ (neutral wino), and the two neutral higgsinos, $\tilde{H}_1^0$, $\tilde{H}_2^0$, while the charged wino $\tilde{W}^\pm$ and the charged higgsino $\tilde{H}^\pm$ constitute the chargino sector. The neutralinos, charginos, and sleptons are color singlet and renormalization-group analyses imply that they are lighter than the others. This characteristics of the superparticle mass spectrum makes an e^+e^- collider a useful machine to search for the superparticles. The "first superparticle" in the e^+e^- collider will then be a slepton or a chargino. Occasionally a scalar top quark may be light and the first signal due to a large left-right mixing in the mass matrix, but we disregard this possibility in this paper. In any case the first superparticle decays into the LSP which is usually assumed to be a neutralino.

Next we discuss the masses of the superparticles. For our present purposes, it is sufficient to consider those of the neutralinos, charginos, and sleptons. We will first explain the parameter set used in the Monte Carlo simulation. In the minimal supergravity, the soft SUSY breaking parameters are only the following four: a universal scalar mass m_0, a universal gaugino mass $M_{1/2}$, a trilinear scalar coupling A, and B which appears in the Higgs mixing mass term. The slepton masses are parameterized by m_0 and $M_{1/2}$. In order to specify the neutralino and chargino sectors, we need additional two parameters, μ the supersymmetric higgsino mass parameter and $\tan\beta$, the ratio of the vacuum expectation values of the two neutral Higgs scalars. The set of the four parameters[22],

$$m_0,\ M_{1/2},\ \mu,\ \tan\beta \tag{A.1}$$

completely specifies the mass spectrum and interactions of the superparticles we are now concerned with.

The gaugino mass parameters at the electro-weak scale can be given by solving the renormalization-group equations. Under the assumptions of the minimal particle content and the universal gaugino mass at high energy scale, the gaugino mass parameters for the $U(1)_Y$ and $SU(2)_L$ are given by

$$M_1 = \tfrac{5}{3}\tfrac{\alpha'}{\alpha_U} M_{1/2} = 0.42 M_{1/2}, \tag{A.2}$$

$$M_2 = \tfrac{\alpha_2}{\alpha_U} M_{1/2} = 0.82 M_{1/2}, \tag{A.3}$$

respectively. Here α_U is the gauge coupling at the unification scale. Note that the mass relation

$$\frac{M_1}{M_2} = \frac{5}{3}\tan^2\theta_W = 0.50 \tag{A.4}$$

holds for any GUT model at the one-loop level of the renormalization-group equations as long as the gauge group is unified into a simple group and the gaugino mass is universal at the GUT scale[23]. Therefore Eq. (A.4) is called the GUT-relation for the gaugino masses. The mass matrix of the neutralinos is written as

$$\begin{pmatrix} M_1 & 0 & -m_Z\sin\theta_W\cos\beta & m_Z\sin\theta_W\sin\beta \\ 0 & M_2 & m_Z\cos\theta_W\cos\beta & -m_Z\cos\theta_W\sin\beta \\ -m_Z\sin\theta_W\cos\beta & m_Z\cos\theta_W\cos\beta & 0 & -\mu \\ m_Z\sin\theta_W\sin\beta & -m_Z\cos\theta_W\sin\beta & -\mu & 0 \end{pmatrix}, \tag{A.5}$$

on the $(\tilde{B}, \tilde{W}^3, \tilde{H}_1^0, \tilde{H}_2^0)$ basis. The mass eigenstates can be obtained by diagonalizing the mass matrix. The resulting mass eigenstates are denoted as $\tilde{\chi}_i^0$ $(i = 1,2,3,4)$ with masses $m_{\tilde{\chi}_1^0} < \cdots < m_{\tilde{\chi}_4^0}$. Similarly the chargino mass matrix is given as

$$\begin{pmatrix} M_2 & \sqrt{2}m_W\cos\beta \\ \sqrt{2}m_W\sin\beta & \mu \end{pmatrix}. \tag{A.6}$$

We denote the lighter and the heavier charginos as $\tilde{\chi}_1^\pm$ and $\tilde{\chi}_2^\pm$, respectively.

The GUT-relation for the gaugino masses was imposed in our Monte Carlo event generations and in many of our analyses. But we also showed that the global fit discussed in Section 2.3 allows us to determine the masses of M_1 and M_2 independently and to test if Eq. (A.4) is satisfied. If discrepancy from it is observed, the idea of the SUSY-GUT will run into serious trouble.

The slepton masses are also given as the solutions of the renormalization-group equations. In the minimal supergravity scenario, they are written in the form:

$$m_{\tilde{l}_R}^2 = m_0^2 + 0.15 M_{1/2}^2 - \sin^2\theta_W m_Z^2\cos 2\beta, \tag{A.7}$$

$$m_{\tilde{l}_L}^2 = m_0^2 + 0.52 M_{1/2}^2 - \frac{1}{2}(1 - 2\sin^2\theta_W) m_Z^2\cos 2\beta, \tag{A.8}$$

$$m_{\tilde{\nu}_L}^2 = m_0^2 + 0.52 M_{1/2}^2 + \frac{1}{2} m_Z^2\cos 2\beta. \tag{A.9}$$

The first terms are the boundary conditions at the GUT scale which are taken to be common under the assumption of the universal scalar mass, the second terms come from the renormalization-group effects, and the third ones are contributions from the D-terms which arise at the electro-weak symmetry breaking.

As was mentioned previously, we used the above formulas of the slepton masses in the Monte Carlo simulation. If we relax the assumption of the universal scalar mass, the above relations will no longer hold. For example, in the $SU(5)$ GUT with the minimal particle content below the GUT scale, we have

$$m_{\tilde{l}_R}^2 = m_{10}^2 + 0.15 M_{1/2}^2 - \sin^2\theta_W m_Z^2\cos 2\beta - 0.053 S, \tag{A.10}$$

$$m^2_{\tilde{l}_L} = m^2_{\mathbf{5}^*} + 0.52M^2_{1/2} - \frac{1}{2}(1 - 2\sin^2\theta_W)m^2_Z \cos 2\beta + 0.027S, \quad (A.11)$$

$$m^2_{\tilde{\nu}_L} = m^2_{\mathbf{5}^*} + 0.52M^2_{1/2} + \frac{1}{2}m^2_Z \cos 2\beta + 0.027S, \quad (A.12)$$

where S is defined by

$$S = m^2_2 - m^2_1 + \sum_{generations}(m^2_{\tilde{q}} - 2m^2_{\tilde{u}} + m^2_{\tilde{e}} - m^2_{\tilde{l}} + m^2_{\tilde{d}}), \quad (A.13)$$

which is evaluated at the GUT scale. Here m^2_1 and m^2_2 stand for the soft SUSY breaking mass terms of the Higgs bosons with hypercharge $-1/2$ and $+1/2$, respectively. In the $SU(5)$ GUT, it becomes simply

$$S = m^2_2 - m^2_1. \quad (A.14)$$

Note that S vanishes under the assumption of the universal scalar mass. From the $SU(5)$ symmetry alone, $m_{\mathbf{10}}$ and $m_{\mathbf{5}^*}$ may be different. These could be even generation-dependent. Note that, on the other hand, the mass difference of the doublet

$$m^2_{\tilde{l}_L} - m^2_{\tilde{\nu}_L} = -(1 - \sin^2\theta_W)m^2_Z \cos 2\beta \quad (A.15)$$

is just the D-term contribution and is model-independent.

These slepton mass relations can be used in a variety of ways. (a) In the $SU(5)$ GUT, one can measure the difference

$$m^2_{\tilde{l}_L} - m^2_{\tilde{l}_R} = m^2_{\mathbf{5}^*} - m^2_{\mathbf{10}} + 0.37M^2_\infty - \frac{1}{2}(1 - 4\sin^2\theta_W)m^2_Z \cos 2\beta + 0.080S, \quad (A.16)$$

and its dependence on β is extremely weak thanks to an accidental cancellation $1 - 4\sin^2\theta_W \simeq 0.07$. Assuming that the contribution from S is also negligible, a precise determination of left-handed and right-handed slepton masses measures the difference between $m^2_{\mathbf{10}}$ and $m^2_{\mathbf{5}^*}$. (b) Once we know $m^2_{\tilde{\nu}_L}$ from the t-channel exchange in the chargino pair production, we can set an upper bound on the $m^2_{\tilde{l}_L}$ without assuming the GUT-relation nor the minimal supergravity. (c) If we know $m^2_{\tilde{l}_R}$ and M_2 from the right-handed slepton and the chargino/neutralino studies, we can set an upper bound on $m^2_{\tilde{l}_L}$ assuming the universal scalar mass. Since the sensitivity to the t-channel sneutrino exchange is weak for a higgsino-dominant chargino, this may be also a useful tool to set the next target energy in this case.

B Monte Carlo Simulation

In our Monte Carlo simulations, we assumed the universal scalar mass at the GUT scale. Then the masses and the interactions of the neutralinos, the charginos, and the sleptons are parameterized by

$$m_0, M_2, \mu, \tan\beta. \quad (A.17)$$

We followed the convention of [24] in translating these parameters into particle masses and couplings. As for the standard model parameters, we have used $\alpha = 1/128$, $\sin^2\theta_W = 0.230$, $m_W = 80$ GeV, and $m_Z = 91.17$ GeV.

The Monte Carlo data used in this paper were generated as follows for both signal and background events. First we calculated, at the tree level, full helicity amplitudes including decays into final-state partons, using the HELAS library[25], which allows us to implement correct angular correlations and effects of the natural widths of unstable partons such as W and Z: our amplitudes for the background processes such as $e^+e^- \to e^\pm \overset{(-)}{\nu_e} W^\mp$, $e^+e^-W^+W^-$, *etc* are thus exact, not based on the equivalent particle approximation. With this scheme, it is also easy to handle polarized beams.

The effective cross sections were then evaluated by the numerical integration package BASES[26], taking into account the effects of initial state radiation, beam energy spread, and beamstrahlung[27]. We have used the formula in [28] for the initial state radiation. The beam energy before beamstrahlung was assumed to have a flat distribution with a width of 1.0 % in FWHM and that after the beamstrahlung was calculated by the formulas given in [29]. The input parameters to the formulas are the nominal beam energy (E^0), the number of particles in a single beam bunch (N), and the root-mean-square sizes of the beam (σ_x, σ_y, and σ_z). We have used $E^0 = 150$ GeV, $N = 0.63 \times 10^{10}$, $\sigma_x = 0.335$ μm, $\sigma_y = 0.00392$ μm, and $\sigma_z = 85$ μm for the simulations at $\sqrt{s} = 350$ and 400 GeV. For the simulations at $\sqrt{s} = 500$ GeV, we have switched the parameters to $E^0 = 250$ GeV, $N = 0.63 \times 10^{10}$, $\sigma_x = 0.260$ μm, $\sigma_y = 0.00304$ μm, and $\sigma_z = 67$ μm. These beam-related parameters were cited from [4].

The BASES integration package enables us to generate four-momenta of final-state partons, once the integration is completed.

When these partons involved quarks, we used the LUND parton shower and string fragmentation programs[30]. The generated events were then processed through a detector simulator, in order to take into account the effects of the geometric acceptance and resolutions of our model detector described in [4]. The main detector components used in the analyses are the central drift chamber (CDC), the electromagnetic (EMC) and the hadron calorimeters (HDC), and the muon drift chamber. It should be noted that we tried to link charged particles detected in the CDC to energy clusters detected in the EMC or HDC, and, when linked, we used the CDC information, since it has better resolution in general. To be realistic in this linking process, we generated calorimeter hits with a finite shower size and simulated the cluster overlapping.

References

[1] M. Zolotarev, E. Kuraev, and V. Serbo, Inst. Yadernoi Fiziki Preprint 81-63 (1981); SLAC TRANS-227 (1987); P. Chen and V. Telnov, *Phys. Rev. Lett.* **63** (1989) 1796; T. Tauchi, K. Yokoya, and P. Chen, *Particle Acc.* **41** (1993) 29.

[2] M. Drees and R. Godbole, DESY-92-044, Mar (1992).

[3] C. Ahn *et al*, SLAC-0329 (1988).

[4] JLC Group, KEK-Report 92-16 (1992).

[5] *Proceedings of the First JLC Workshop*, KEK, Oct. 24-25 (1989); *Proceedings of the Second JLC Workshop*, KEK, Nov. 6-8 (1990); *Proceedings of the Third JLC Workshop*, KEK, Feb. 18-20 (1992).

[6] T. Maruyama *et al*, *Phys. Rev. Lett.* **66** (1991) 2351.

[7] T. Omori *et al*, *Phys. Rev. Lett.* **67** (1991) 3294; T. Nakanishi *et al*, *Phys. Lett.* **A158** (1991) 345; H. Aoyagi *et al*, *Phys. Lett.* **A167** (1992) 415;

[8] ALEPH, DELPHI, L3, and OPAL, *Phys. Lett.* **B276** (1992) 247.

[9] In the energy region of our interest, we can approximate Z to be massless and assume the $SU(2)_L \times U(1)_Y$ symmetry limit. In this limit, the $\tilde{e}_R$ pair production takes place via the annihilation into the $U(1)_Y$ gauge boson B. The signal cross section is thus enhanced, since right-handed electrons have a larger hyper charge than that of left-handed ones. On the other hand, the W^+W^- production is absent for the right-handed beam in the symmetry limit, since its s-channel diagram only involves the annihilation into the neutral $SU(2)_L$ gauge boson W^0 and its t-channel diagram has the exchange of the electron neutrino. As for the $e^{\pm}\overset{(-)}{\nu_e}W^{\mp}$ background, the right-handed electron eliminates diagrams with a t-channel W exchange between the initial-state e^+ and e^- which turned out to contribute dominantly after the angle cuts defined above.

[10] There are possibilities which invalidate the GUT-relation of the gaugino masses even within the SUSY-GUT. First, the threshold corrections at the GUT-scale may induce non-universal contributions to the three gaugino masses (T. Goto, J. Hisano, and H. Murayama, TU-432 (1993), to appear in *Phys. Rev.* **D**). Second, the two-loop contribution to the renormalization group equations of gaugino masses destroy the universality (Y. Yamada, *Phys. Lett.* **B336**, 109 (1993); KEK-TH-371 (1993); S. Martin and M. Vaughn, NUB-3072-93-TH (1993)). These two effects are usually small, but may be large in special circumstances, for instance, when A or B is much larger than the gaugino mass. Finally, there may be higher dimension operators which break the universality. This contribution is suppressed by M_{GUT}/M_{Planck}, but may be large if the universal contribution is somehow small, or M_{GUT} is close to M_{Planck}.

[11] Since our parameter set gives a bino-dominant $\tilde{\chi}_1^0$ and a wino-dominant $\tilde{\chi}_2^0$, the left-handed electron beam is preferred from the view point of coupling strength. The left-handed electron beam, however, requires the t-channel exchange of $\tilde{e}_L$ which is significantly heavier than $\tilde{e}_R$ here. Because of this propagator suppression and the smallness of hyper charge, the cross section for the left-handed electron beam is not very much different from that for the right-handed electron beam.

[12] A. Miyamoto, *Proceedings of the Second JLC Workshop*, KEK, Nov. 6-8 (1990) 256.

[13] We assumed here that we can determine the charge of at least one W candidate in a reconstructed event by using, for instance, the charge of a lepton from charm decay or the reconstruction of a charmed meson or both.

[14] In our choice of parameters, the global fit can be understood roughly as follows. First, the chargino is little produced from the right-handed beam, and we obtain an upper bound on its higgsino component. On the other hand, the t-channel neutralino exchange in $\sigma_R(\tilde{e}_R)$ is consistent with the assumption that the LSP is nearly a pure bino. Then we can translate the chargino and the LSP masses to M_2 and M_1. In Fig.13, one observes that the resultant M_1 and M_2 are different from the input $m_{\tilde{\chi}_1^0}$ and $m_{\tilde{\chi}_1^\pm}$; the difference represents the contamination from the higgsino component.

[15] Note that this upper bound is obtained without assuming boundary conditions at the GUT or Planck scales. It can be derived solely from the weak-scale supersymmetric Lagrangian.

[16] This center-of-mass energy is actually lower than the chargino-pair threshold, which is specific to our choice of parameters. The associate $\tilde{e}_L\tilde{e}_R$ production should have been already observed when we studied associate $\tilde{\chi}_1^0\tilde{\chi}_2^0$ production in Section 2.2. Though the cross section for $\tilde{\chi}_1^0\tilde{\chi}_2^0$ is much lower than $\tilde{e}_L\tilde{e}_R$, the signals of these two processes can be separated since $\tilde{e}_L$ decays only into an electron while $\tilde{\chi}_2^0$ has both $e^+e^-\tilde{\chi}_1^0$ and $\mu^+\mu^-\tilde{\chi}_1^0$ modes.

[17] There may be overlaps in the scatter plot between the $\tilde{e}_R$-pair and the $\tilde{e}_R\tilde{e}_L$ associate productions for a different combination of masses. Then a useful observable is the asymmetry of the events with $E_{e^-} > E_{e^+}$ and $E_{e^+} > E_{e^-}$. Once the asymmetry is found, we can extract $m_{\tilde{e}_L}$ from the electron and the positron energy distributions since we already know $m_{\tilde{e}_R}$ and $m_{\tilde{\chi}_1^0}$.

[18] It is an interesting possibility to check the radiative breaking scenario (K. Inoue, A. Kakuto, and H. Takano, *Prog. Theor. Phys.* **68** (1982) 927; L. Ibanez and G. Ross, *Phys. Lett.* **B110** (1982) 215; L. Alvarez-Gaumé, J. Polchinski, and M. Wise, *Nucl. Phys.* **B221** (1983) 495). This requires a detailed study of the Higgs sector, including both light and heavy ones.

[19] We assumed here that the two-body mode has been searched for and not found, which justifies the application of the mass cut to eliminate W's.

[20] If we know $\tan\beta$ from the Higgs sector, then we can further vary M_1 and M_2 independently to test the GUT-relation at this stage.

[21] J. Grivaz, *Physics and Experiments with Linear Colliders*, ed. P. Orava, P. Eerola, and M. Nordberg, World Scientific (1992) 353.

[22] In Section 2, we used the $SU(2)_L$ gaugino mass parameter M_2 instead of $M_{1/2}$. The relation between these two is given by the renormalization-group equations (see Eq. (A.3)).

[23] Y. Kawamura, H. Murayama, and M. Yamaguchi, TU-439 (1993).

[24] K. Hikasa, *JLC SUSY Manual*, in preparation.

[25] H. Murayama, I. Watanabe, and K. Hagiwara, KEK Preprint 91-11 (1992).

[26] S. Kawabata, *Comp. Phys. Comm.* **41** (1986) 127.

[27] We did not include the initial state radiation and the beam effects for the background from the fusion processes: $e^+e^- \to e^+e^-W^+W^-$, $e^\pm \overset{(-)}{\nu_e} W^\mp Z^0$, and $\nu_e\bar{\nu}_e W^+W^-$. Since both the initial state radiation and the beam effects make the cross sections for these processes smaller, our background estimation is conservative.

[28] F. Berends, *Z Physics at LEP-I*, CERN Yellow Report No.89-08, vol.1.

[29] K. Yokoya, *Proceedings of 1988 Linear Accelerator Conference*, CEBAF-Report-89-001 (1989) 494.

[30] T. Sjöstrand and M. Bengtsson, *Comp. Phys. Comm.* **43** (1987) 367.

Table Captions

Table 1 The observables in the right-handed slepton pair production.

Table 2 The physics implications of the observables in the right-handed slepton pair production.

Table 3 The observables in the chargino pair production.

Table 4 The physics implications of the observables in the chargino pair production.

Table 5 The observables in the slepton associate production.

Table 6 The physics implications of the observables in the slepton associate production.

Tables

Table 1:

$m_{\tilde{e}_R}$, $m_{\tilde{\chi}_1^0}$, $m_{\tilde{\mu}_R}$, $\sigma_L(\tilde{e}_R)$, $\sigma_R(\tilde{e}_R)$, $\sigma_L(\tilde{\mu}_R)$, $\sigma_R(\tilde{\mu}_R)$, angular distributions

Table 2:

Upper bound on lighter chargino mass	$m_{\tilde{\chi}_1^0}$
Test of universal scalar mass	$m_{\tilde{e}_R}$, $m_{\tilde{\mu}_R}$
Check of the slepton quantum numbers	$\sigma_L(\tilde{e}_R)$, $\sigma_L(\tilde{\mu}_R)$, $\sigma_R(\tilde{\mu}_R)$
Constraints on neutralino parameters	$m_{\tilde{e}_R}$, $\sigma_R(\tilde{e}_R)$, $m_{\tilde{\chi}_1^0}$, $d\sigma_R(\tilde{e}_R)/d\cos\theta$

Table 3:

$m_{\tilde{\chi}_1^\pm}$, $\sigma_L(\tilde{\chi}_1^\pm)$, $\sigma_R(\tilde{\chi}_1^\pm)$, angular distributions

Table 4:

Higgsino content of $\tilde{\chi}_1^\pm$	$m_{\tilde{\chi}_1^\pm}$, $\sigma_R(\tilde{\chi}_1^\pm)$, angular distribution
Test on GUT-relation of gaugino masses	$m_{\tilde{\chi}_1^\pm}$, $\sigma_R(\tilde{\chi}_1^\pm)$, angular distribution, $\sigma_R(\tilde{e}_R)$, $m_{\tilde{\chi}_1^0}$
Sneutrino mass	$\sigma_R(\tilde{\chi}_1^\pm)$, angular distribution

Table 5:

$m_{\tilde{e}_L}$, $\sigma_R(\tilde{e}_R^-\tilde{e}_L^+)$, $\sigma_L(\tilde{e}_L^-\tilde{e}_R^+)$, angular distributions

Table 6:

universal scalar mass	$m_{\tilde{e}_R}$, $m_{\tilde{e}_L}$, M_2
neutralino sector consistency	$\sigma_R(\tilde{e}_R^-\tilde{e}_L^+)$, $\sigma_L(\tilde{e}_L^-\tilde{e}_R^+)$, angular distributions
conservation of chirality	absence of $\sigma_R(\tilde{e}_L^-\tilde{e}_R^+)$, $\sigma_L(\tilde{e}_R^-\tilde{e}_L^+)$

Figure Captions

Fig. 1 Feynman diagrams for the right-handed slepton-pair productions.

Fig. 2 Total cross sections for slepton productions: (a) $e^+e^- \to \tilde{e}_R^+\tilde{e}_R^-$, $e^+e^- \to \tilde{e}_L^\pm\tilde{e}_R^\mp$, and $e^+e^- \to \tilde{e}_L^+\tilde{e}_L^-$, (b) $e^+e^- \to \tilde{\mu}_R^+\tilde{\mu}_R^-$ and $e^+e^- \to \tilde{\mu}_L^+\tilde{\mu}_L^-$, where dashed, solid, and dotted lines correspond to electron beam polarizations of -1, 0, and $+1$, respectively. The cross sections were evaluated at the lowest order, without including initial state radiation nor beam effects.

Fig. 3 Acoplanarity angle distributions for final-state leptons from right-handed slepton-pair productions (solid) at $\sqrt{s} = 350$ GeV with an integrated luminosity of 20 fb^{-1} after including the initial state radiation and the beamstrahlung effects: (a) $e^+e^- \to \tilde{e}_R^+\tilde{e}_R^-$ with $P_{e^-} = 0$, (b) $e^+e^- \to \tilde{\mu}_R^+\tilde{\mu}_R^-$ with $P_{e^-} = 0$, and (c) $e^+e^- \to \tilde{\mu}_R^+\tilde{\mu}_R^-$ with $P_{e^-} = +0.95$. The dashed lines indicate the W^+W^- background, while the dotted line represents that from the $e^\pm \overset{(-)}{\nu}_e W^\mp$ process.

Fig. 4 (a) The energy distribution of final-state muons for $e^+e^- \to \tilde{\mu}_R^+\tilde{\mu}_R^-$ at $\sqrt{s} = 350$ GeV with an integrated luminosity of 20 fb^{-1} and an electron beam polarization of $P_{e^-} = +0.95$, after including the initial state radiation and the beamstrahlung effects. The smooth curve in the figure is the best-fit curve resulting from a two-parameter fit varying the $\tilde{\mu}_R$ and the $\tilde{\chi}_1^0$ masses. (b) Contours showing the errors on $m_{\tilde{\mu}_R}$ and $m_{\tilde{\chi}_1^0}$ expected for the two-parameter fit.

Fig. 5 The angular distribution of $\tilde{\mu}_R^-$'s in $e^+e^- \to \tilde{\mu}_R^+\tilde{\mu}_R^-$ reconstructed from final-state $\mu^\pm$ four-momenta, knowing the $\tilde{\mu}_R$ and $\tilde{\chi}_1^0$ masses and assuming no initial state radiation and no beamstrahlung: (a) with the two solutions unresolved and (b) with the background due to the wrong solutions subtracted. The Monte Carlo data were generated at $\sqrt{s} = 350$ GeV with an integrated luminosity of 20 fb^{-1} and $P_{e^-} = 0.95$ and plotted without acceptance correction. The histogram in (a) is the distribution of the right solutions, while that in (b) is the distribution of the original sample before selection cuts.

Fig. 6 Similar plots to Figs.5-a) and -b) for $e^+e^- \to \tilde{e}_R^+\tilde{e}_R^-$.

Fig. 7 The upper limits on (a) $m_{\tilde{\chi}_1^\pm}$ and (b) $m_{\tilde{\chi}_2^0}$ as functions of $m_{\tilde{\chi}_1^0}$ assuming the GUT relation on the gaugino masses. The limits become $2.0 \times m_{\tilde{\chi}_1^0}$ in the high $m_{\tilde{\chi}_1^0}$ region, as indicated by dashed lines.

Fig. 8 The $\Delta\chi^2 = 1$ contour in the $m_{\tilde{\mu}_R}$-$m_{\tilde{e}_R}$ plane obtained from fits to the final-state lepton energy distributions for the $\tilde{\mu}_R$- and $\tilde{e}_R$-pair productions. The dotted line corresponds to the universal scalar mass hypothesis.

Fig. 9 Scatter plots of $\mu^\pm$ energies at $\sqrt{s} = 400$ GeV for (a) $e^+e^- \to \tilde{\chi}_1^0\tilde{\chi}_2^0$, (b) $e^+e^- \to W^+W^-$, and (c) $e^+e^- \to \tilde{\mu}_R^+\tilde{\mu}_R^-$, assuming an integrated luminosity of 20 fb^{-1} and an electron beam polarization of $P_{e^-} = +0.95$, and including the initial state radiation

and the beamstrahlung effects. The square boxes in the figures indicate the locations of cuts to select $\tilde{\chi}_1^0\tilde{\chi}_2^0$ events.

Fig. 10 Acoplanarity angle distributions of W pairs from $e^+e^- \to \tilde{\chi}_1^+\tilde{\chi}_1^-$ (solid), $e^+e^- \to W^+W^-$ (dash), $e^+e^- \to e^+e^-W^+W^-$ (dot), and the other background processes: $e^+e^- \to e^{\pm}\overset{(-)}{\nu}_e W^{\mp}Z^0$, $W^+W^-Z^0(\to \nu\bar{\nu})$, and $\nu_e\bar{\nu}_e W^+W^-$ (dot-dash) at $\sqrt{s}$ = 500 GeV with an integrated luminosity of 50 fb^{-1}, after including the initial state radiation and the beamstrahlung effects.

Fig. 11 (a) The energy distribution of W candidates in the final sample defined in the text. The Monte Carlo events include both the signal ($e^+e^- \to \tilde{\chi}_1^+\tilde{\chi}_1^-$) and the background generated at $\sqrt{s}$ = 500 GeV with an integrated luminosity of 50 fb^{-1}, including the initial state radiation and the beamstrahlung effects. The dashed, the dot-dashed, and the dotted curves show the expected shapes of the backgrounds from the W^+W^-, the $e^{\pm}\overset{(-)}{\nu}_e W^{\mp}Z^0$, and the other processes ($W^+W^-Z^0$, $e^+e^-W^+W^-$, $\nu_e\bar{\nu}_e W^+W^-$), respectively, while the solid line is the best-fit curve obtained from a two-parameter ($m_{\tilde{\chi}_1^0}$ and $m_{\tilde{\chi}_1^\pm}$) fit to the energy distribution. The fit takes into account the shapes of the background distributions. (b) The contours resulting from the two-parameter fit.

Fig. 12 (a) An example of the reconstructed production angle distribution (data points) compared with the generated angle distribution of the selected sample (histogram). The Monte Carlo events were generated at $\sqrt{s}$ = 500 GeV and correspond to an integrated luminosity of 50 fb^{-1}. We have assumed a 100% charge ID efficiency for W's here. The production angles were reconstructed from the four-jet final states, knowing the W, the chargino, and the LSP masses and assuming no initial state radiation and no beamstrahlung. The two solutions were plotted in the same figure. (b) Same as (a) but after the subtraction of the background due to wrong solutions. The histogram is the scaled generated angle distribution for the initial sample before selection cuts, while the data points are the reconstructed without acceptance correction.

Fig. 13 The $\Delta\chi^2 = 1$ contour in the M_1-M_2 plane obtained from the global fit explained in the text. The dotted line indicates the GUT prediction: $M_1 = (5/3)\tan^2\theta_W M_2$.

Fig. 14 The total cross section for $e^+e^- \to \tilde{\chi}_1^+\tilde{\chi}_1^-$ at $\sqrt{s}$ = 500 GeV as a function of the mass of the electron sneutrino. The cross section was evaluated at the lowest order without including initial state radiation nor beam effects for an unpolarized electron beam $P_{e^-} = 0$. The dot-dashed curves represent the ± 1-σ bounds from the global fit explained in the text.

Fig. 15 The Feynman diagram for $e^+e^- \to \tilde{e}_L^{\pm}\tilde{e}_R^{\mp}$.

Fig. 16 The branching fraction of $\tilde{e}_L^{\pm}$ into $e^{\pm}\tilde{\chi}_1^0$ in the plane of M_2 and m_0. The shaded regions correspond to the case where the LSP is not the lightest neutralino.

Fig. 17 The scatter plot of $e^{\pm}$ energies at $\sqrt{s}$ = 400 GeV with an integrated luminosity of 20 fb^{-1} and an electron beam polarization of $P_{e^-} = +0.95$ for $e^+e^- \to \tilde{e}_L^{\pm}\tilde{e}_R^{\mp}$ and $e^+e^- \to \tilde{e}_R^+\tilde{e}_R^-$, including the initial state radiation and the beamstrahlung effects.

Fig. 18 (a) The energy distribution of final-state positrons for the candidate $\tilde{e}_L^{\pm}\tilde{e}_R^{\mp}$ events. The Monte Carlo data were generated at $\sqrt{s}$ = 400 GeV for an integrated luminosity of 20 fb^{-1} and $P_{e^-} = +0.95$, after including the initial state radiation and the beamstrahlung effects. The smooth line is the best-fit curve from the two-parameter fit described in the text. (b) The contours from the two-parameter fit.

Fig. 19 The expected $\Delta\chi^2 = 1$ contour in the plane of the squared mass difference of the left-handed and the right-handed selectrons versus M_2^2. The dotted lines represent the universal scalar mass hypothesis for $\tan\beta = 0$ and 30.

Fig. 20 Feynman diagrams for $e^+e^- \to \tilde{\chi}_1^+\tilde{\chi}_1^-$.

Fig. 21 The distribution of acoplanarity angles for the two-jet+lepton final states from the lighter chargino pair productions (solid) at $\sqrt{s}$ = 500 GeV with initial state radiation and the beamstrahlung effects. The dashed and dotted histograms represent the background distributions expected for W^+W^- and $e^{\pm}\overset{(-)}{\nu}_e W^{\mp}$ productions, respectively.

Fig. 22 (a) The energy distribution of the two-jet systems from the lighter chargino decays for Monte Carlo data generated at $\sqrt{s}$ = 500 GeV with an integrated luminosity of 20 fb^{-1}, after including the initial state radiation and the beamstrahlung effects. The data points include both signal and background events. The solid line is the best-fit curve to the distribution, varying $m_{\tilde{\chi}_1^0}$ and $m_{\tilde{\chi}_1^\pm}$. The dashed and the dotted lines indicate, respectively, the expected shapes of the W^+W^- and the $e^{\pm}\overset{(-)}{\nu}_e W^{\mp}$ backgrounds. (b) The resultant contours from the two-parameter fit.

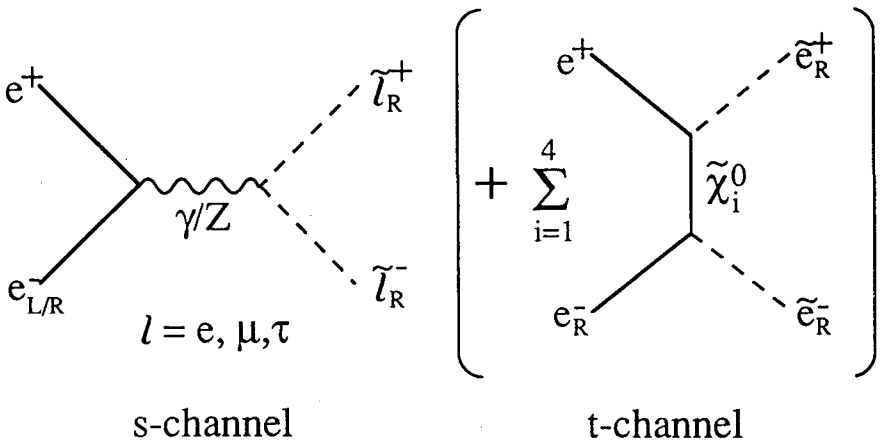
e+
e-L/R
γ/Z
l = e, μ,τ
l+R
l-R
s-channel
+ Σ 4 i=1
e+
e-R
χ̃0i
ẽ+R
ẽ-R
t-channel

Fig.1

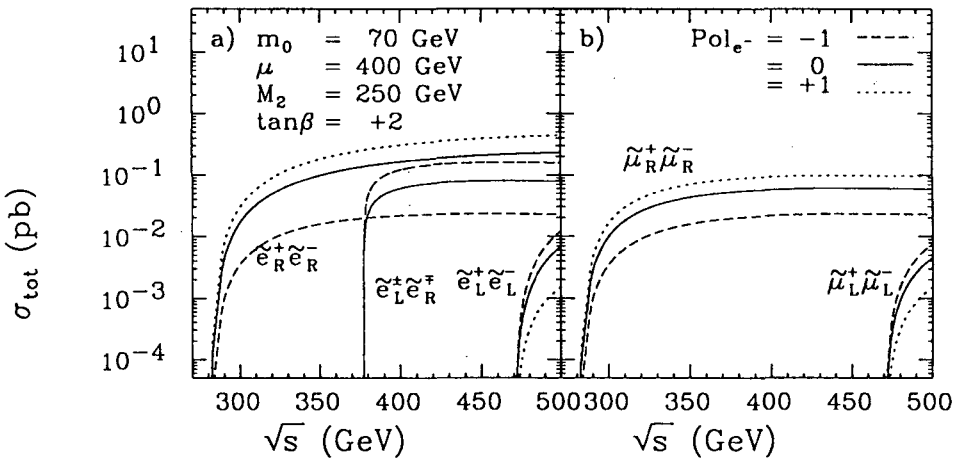
σtot (pb)
a) m0 = 70 GeV
μ = 400 GeV
M2 = 250 GeV
tanβ = +2
b) Pole- = −1
= 0
= +1
μ̃+Rμ̃-R
ẽ+Rẽ-R
ẽ+Lẽ-R
ẽ+Lẽ-L
μ̃+Lμ̃-L
√s (GeV)
√s (GeV)

Fig.2

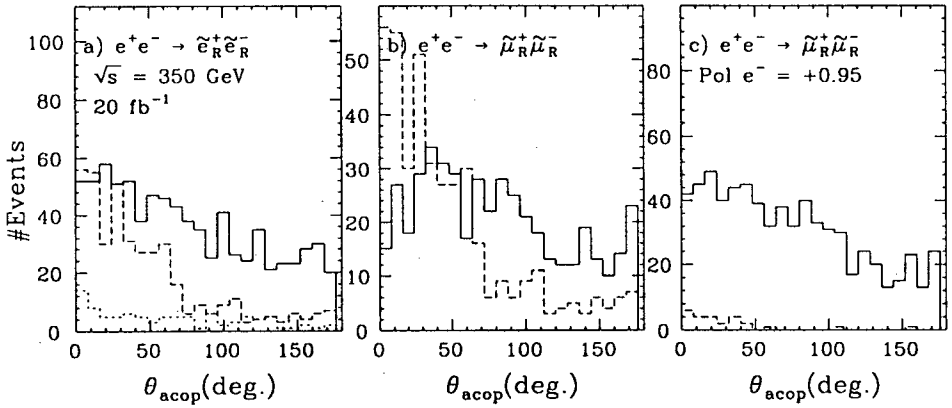
a) $e^+e^- \to \tilde{e}_R^+\tilde{e}_R^-$
$\sqrt{s}$ = 350 GeV
20 fb^{-1}
b) $e^+e^- \to \tilde{\mu}_R^+\tilde{\mu}_R^-$
c) $e^+e^- \to \tilde{\mu}_R^+\tilde{\mu}_R^-$
Pol e^- = +0.95
#Events
θ_{acop}(deg.)

Fig.3

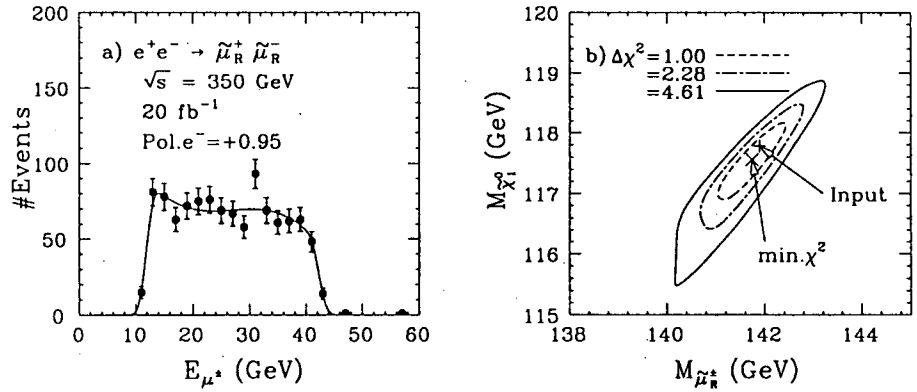
a) $e^+e^- \to \tilde{\mu}_R^+\tilde{\mu}_R^-$
$\sqrt{s}$ = 350 GeV
20 fb^{-1}
Pol.e^-=+0.95
#Events
E_{μ^*} (GeV)
b) $\Delta\chi^2$=1.00
=2.28
=4.61
Input
min.χ^2
$M_{\tilde{\chi}_1^0}$ (GeV)
$M_{\tilde{\mu}_R^*}$ (GeV)

Fig.4

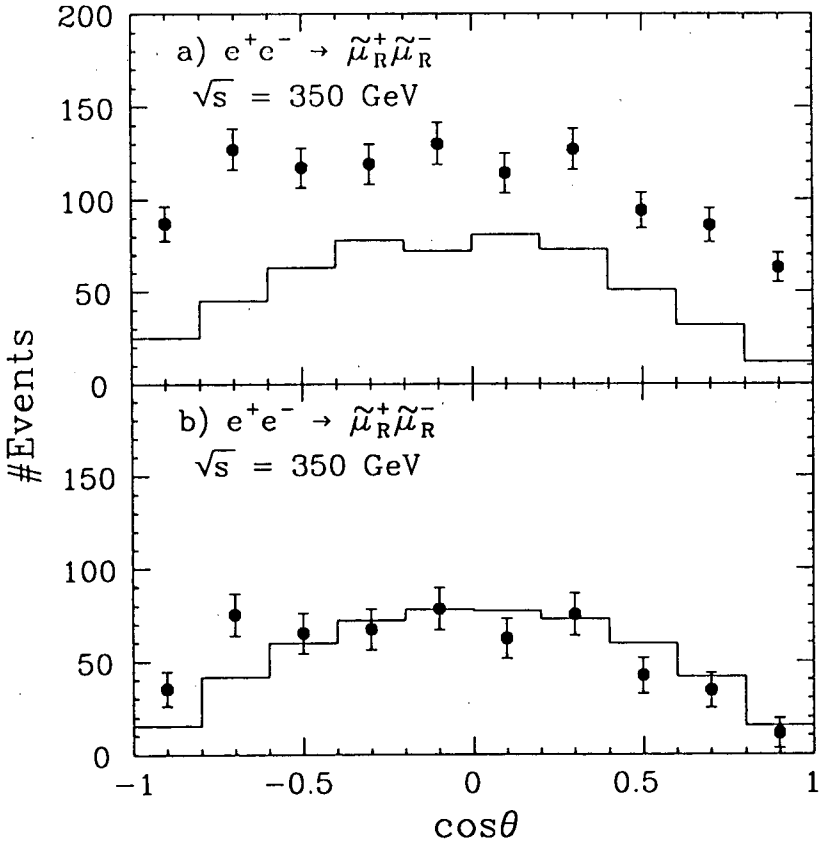
a) $e^+e^- \to \tilde{\mu}_R^+\tilde{\mu}_R^-$
$\sqrt{s}$ = 350 GeV
b) $e^+e^- \to \tilde{\mu}_R^+\tilde{\mu}_R^-$
$\sqrt{s}$ = 350 GeV
#Events
cosθ

Fig.5

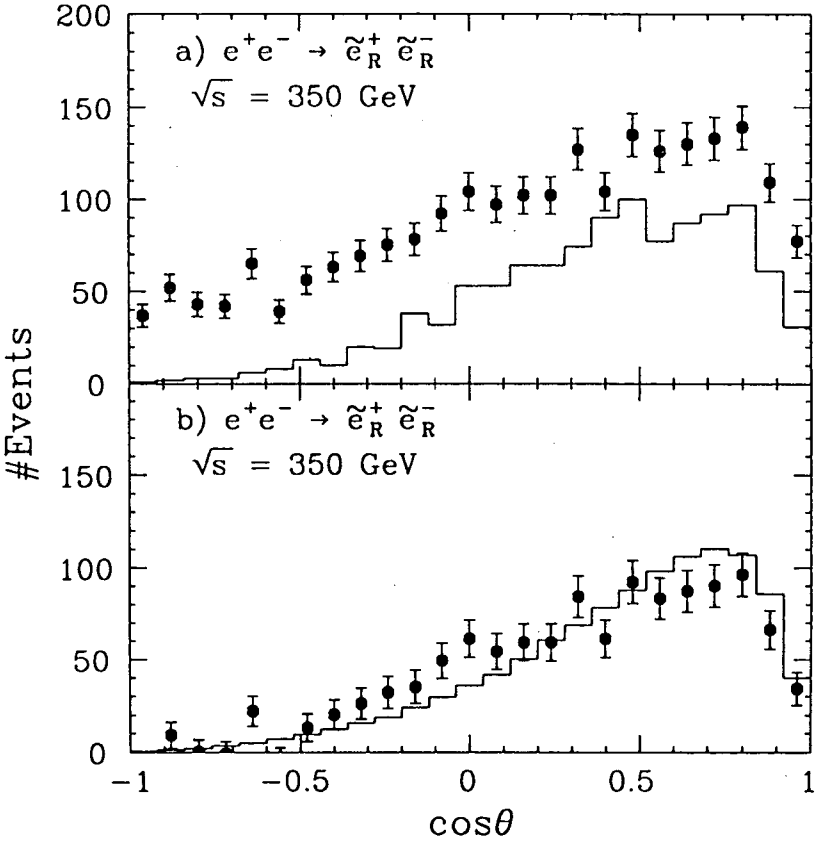
a) $e^+e^- \to \tilde{e}_R^+\tilde{e}_R^-$
$\sqrt{s}$ = 350 GeV
b) $e^+e^- \to \tilde{e}_R^+\tilde{e}_R^-$
$\sqrt{s}$ = 350 GeV
#Events
cosθ

Fig.6

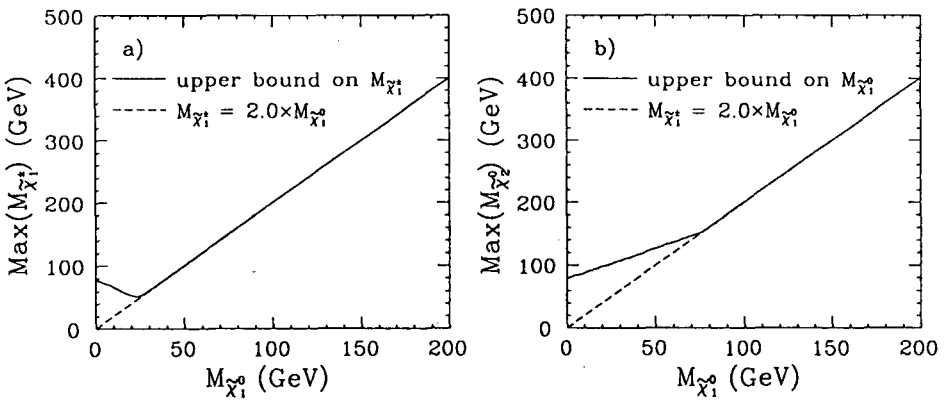
a)
upper bound on $M_{\tilde{\chi}_1^\pm}$
$M_{\tilde{\chi}_1^\pm} = 2.0 \times M_{\tilde{\chi}_1^0}$
$\mathrm{Max}(M_{\tilde{\chi}_1^\pm})$ (GeV)
$M_{\tilde{\chi}_1^0}$ (GeV)
b)
upper bound on $M_{\tilde{\chi}_1^0}$
$M_{\tilde{\chi}_1^\pm} = 2.0 \times M_{\tilde{\chi}_1^0}$
$\mathrm{Max}(M_{\tilde{\chi}_2^0})$ (GeV)
$M_{\tilde{\chi}_1^0}$ (GeV)

Fig.7

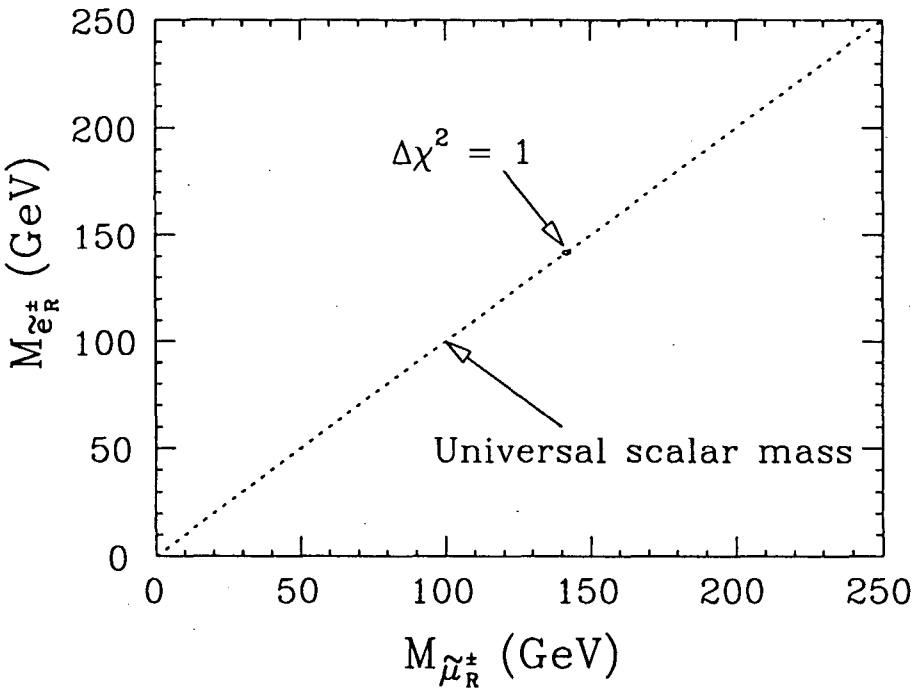
$\Delta\chi^2 = 1$
Universal scalar mass
$M_{\tilde{e}_R^\pm}$ (GeV)
$M_{\tilde{\mu}_R^\pm}$ (GeV)

Fig.8

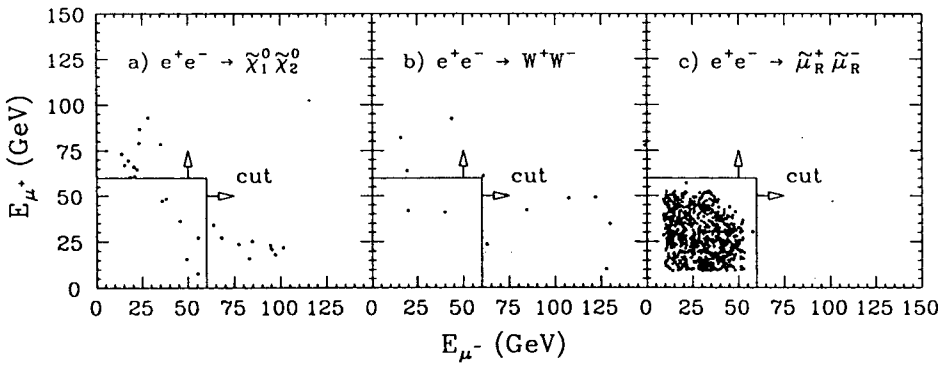
a) $e^+e^- \to \tilde{\chi}_1^0 \tilde{\chi}_2^0$
b) $e^+e^- \to W^+W^-$
c) $e^+e^- \to \tilde{\mu}_R^+ \tilde{\mu}_R^-$
cut
cut
cut
E_{μ^+} (GeV)
E_{μ^-} (GeV)
0 25 50 75 100 125
0 25 50 75 100 125
0 25 50 75 100 125 150
0 25 50 75 100 125 150

Fig.9

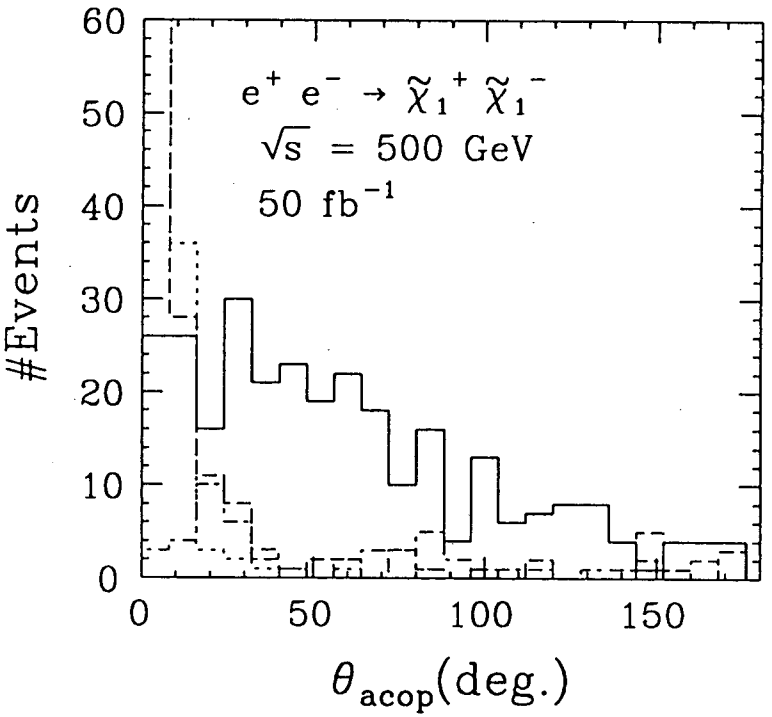
$e^+ e^- \to \tilde{\chi}_1^+ \tilde{\chi}_1^-$
$\sqrt{s}$ = 500 GeV
50 fb^{-1}
#Events
θ_{acop}(deg.)
0 10 20 30 40 50 60
0 50 100 150

Fig.10

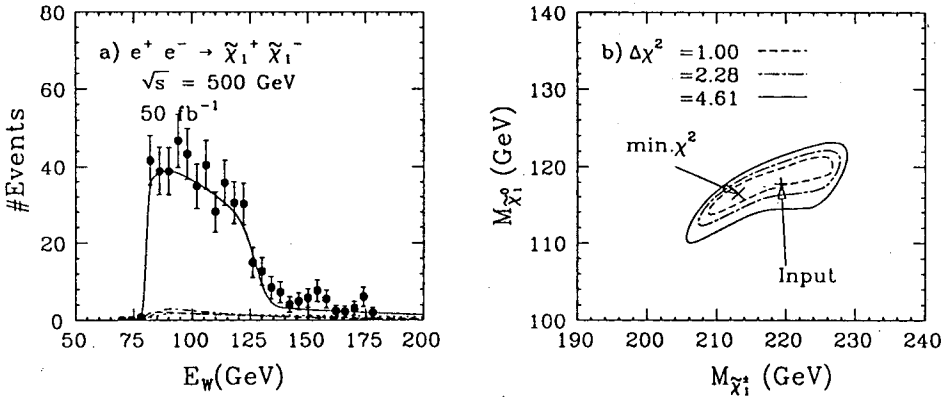
a) e+ e− → χ̃1+ χ̃1−
√s = 500 GeV
50 fb−1
#Events
E_W(GeV)
b) Δχ² =1.00
=2.28
=4.61
min.χ²
Input
M_χ̃1⁰ (GeV)
M_χ̃1± (GeV)

Fig.11

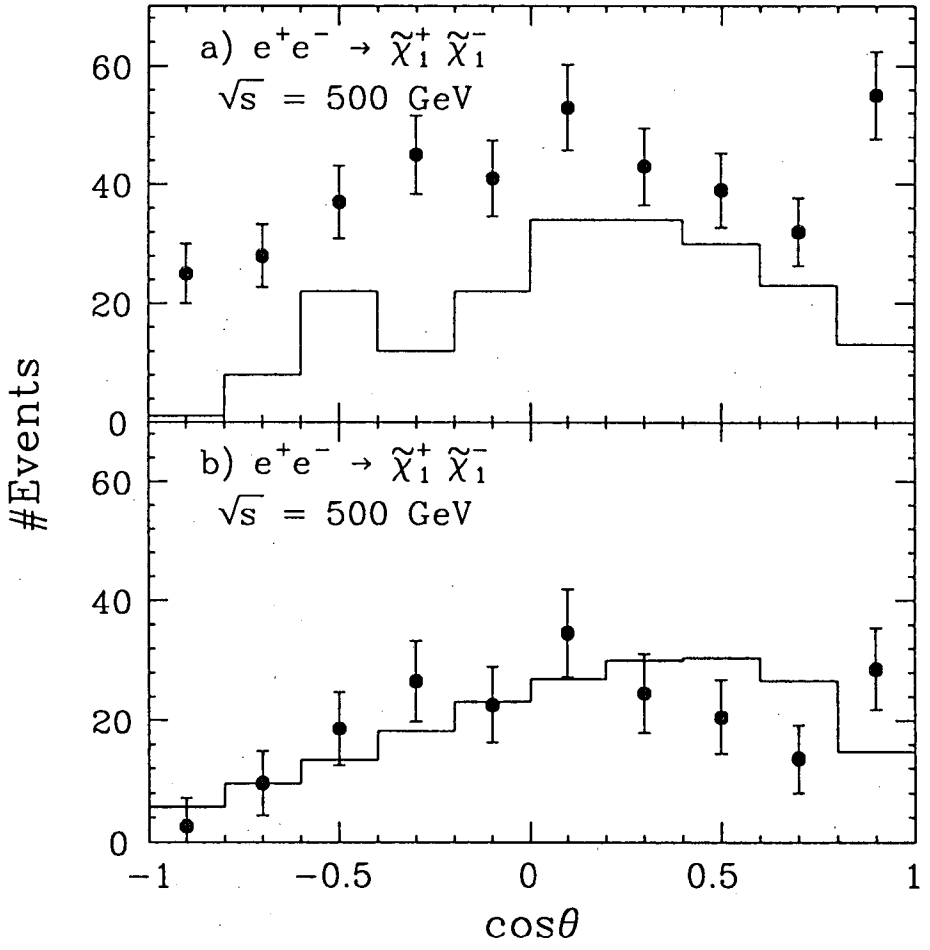
a) e+e− → χ̃1+ χ̃1−
√s = 500 GeV
b) e+e− → χ̃1+ χ̃1−
√s = 500 GeV
#Events
cosθ

Fig.12

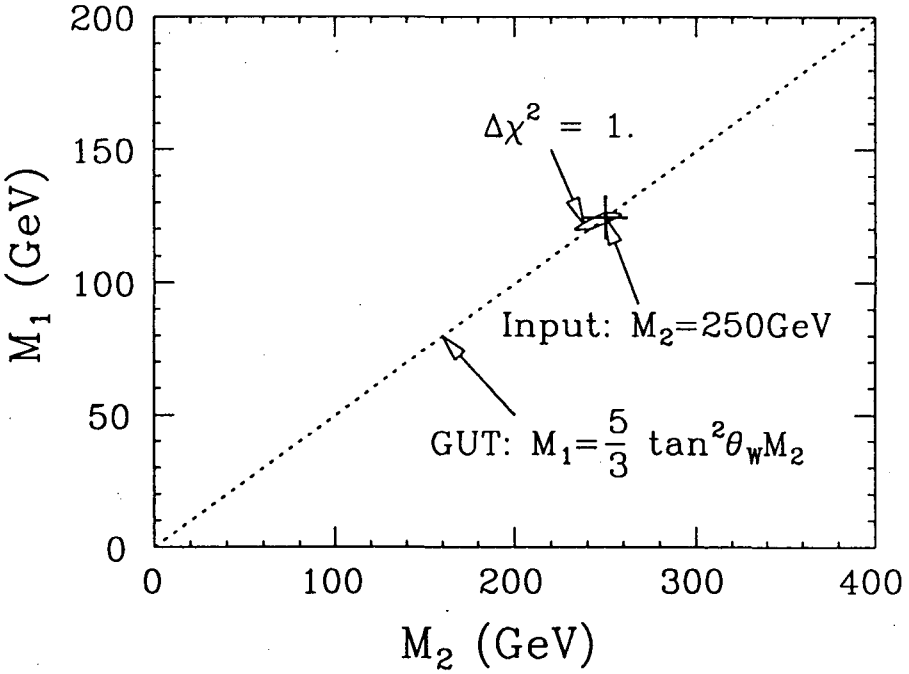
200
150
100
50
0
0
100
200
300
400
M_1 (GeV)
M_2 (GeV)
$\Delta\chi^2 = 1.$
Input: M_2=250GeV
GUT: $M_1=\frac{5}{3}\tan^2\theta_W M_2$

Fig.13

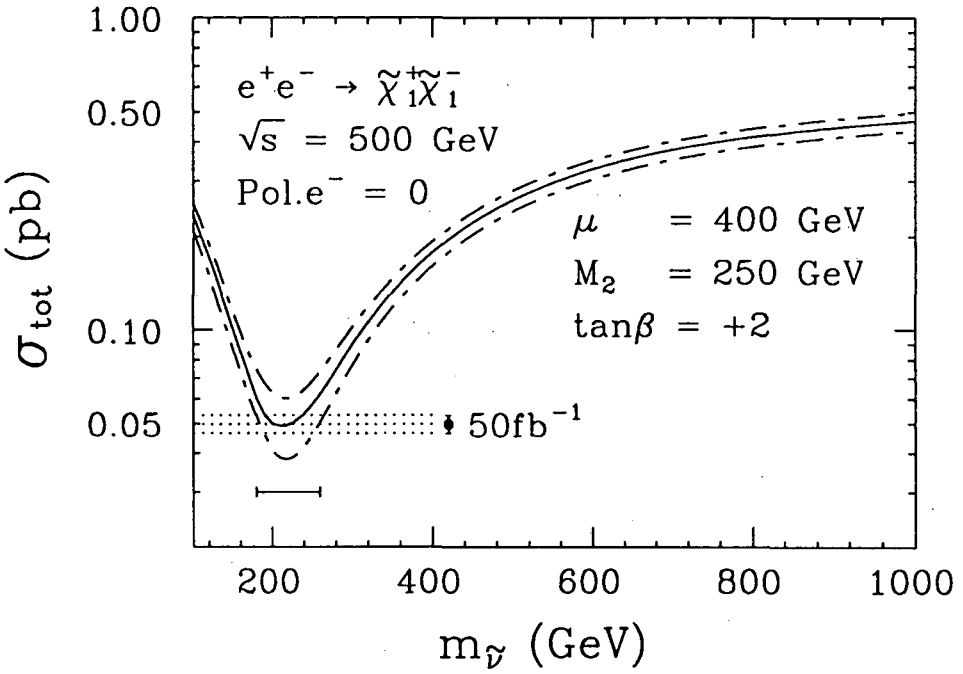
1.00
0.50
0.10
0.05
200
400
600
800
1000
σ_{tot} (pb)
$m_{\tilde{\nu}}$ (GeV)
$e^+e^- \to \tilde{\chi}_1^+\tilde{\chi}_1^-$
$\sqrt{s}$ = 500 GeV
Pol.e^- = 0
μ = 400 GeV
M_2 = 250 GeV
tanβ = +2
50fb^{-1}

Fig.14

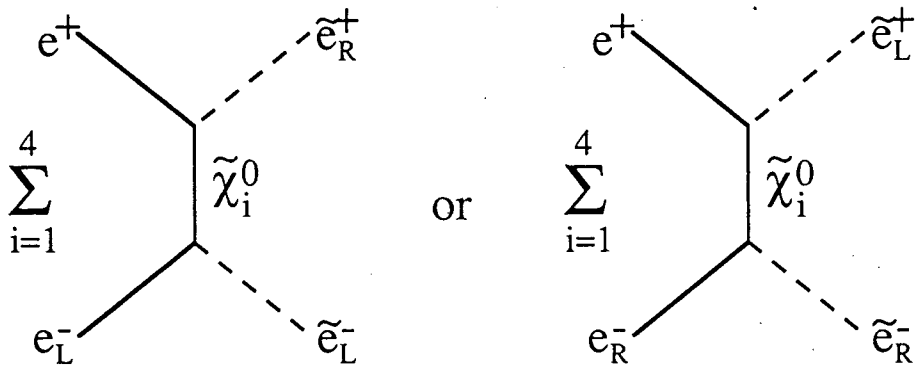
e+
$\tilde{e}_R^+$
$\sum_{i=1}^{4}$
$\tilde{\chi}_i^0$
e_L^-
$\tilde{e}_L^-$
or
e+
$\tilde{e}_L^+$
$\sum_{i=1}^{4}$
$\tilde{\chi}_i^0$
e_R^-
$\tilde{e}_R^-$

Fig.15

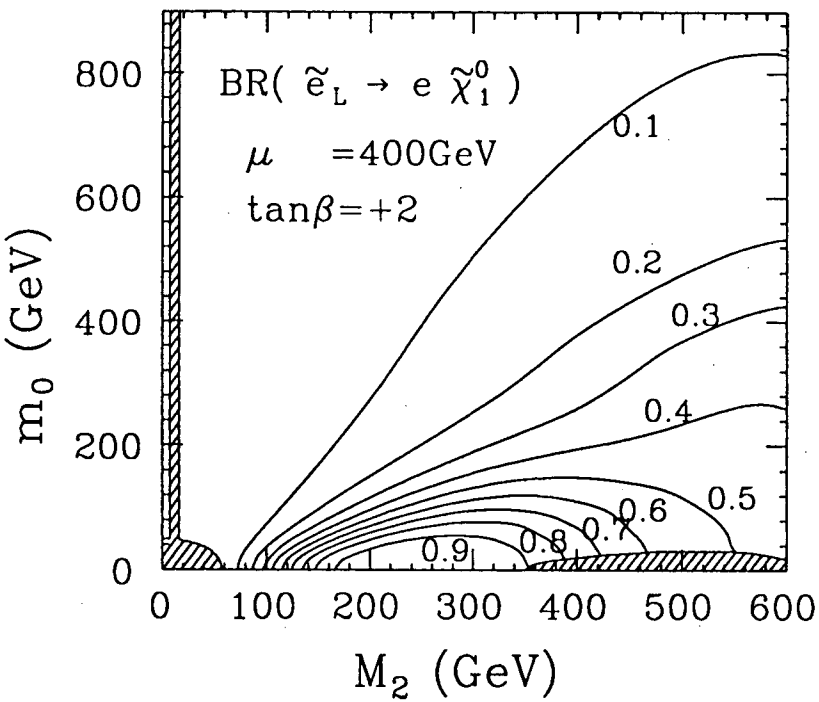
BR($\tilde{e}_L \rightarrow e\ \tilde{\chi}_1^0$)
μ =400GeV
tanβ=+2
0.1
0.2
0.3
0.4
0.5
0.6
0.7
0.8
0.9
m_0 (GeV)
M_2 (GeV)
0
200
400
600
800
0
100
200
300
400
500
600

Fig.16

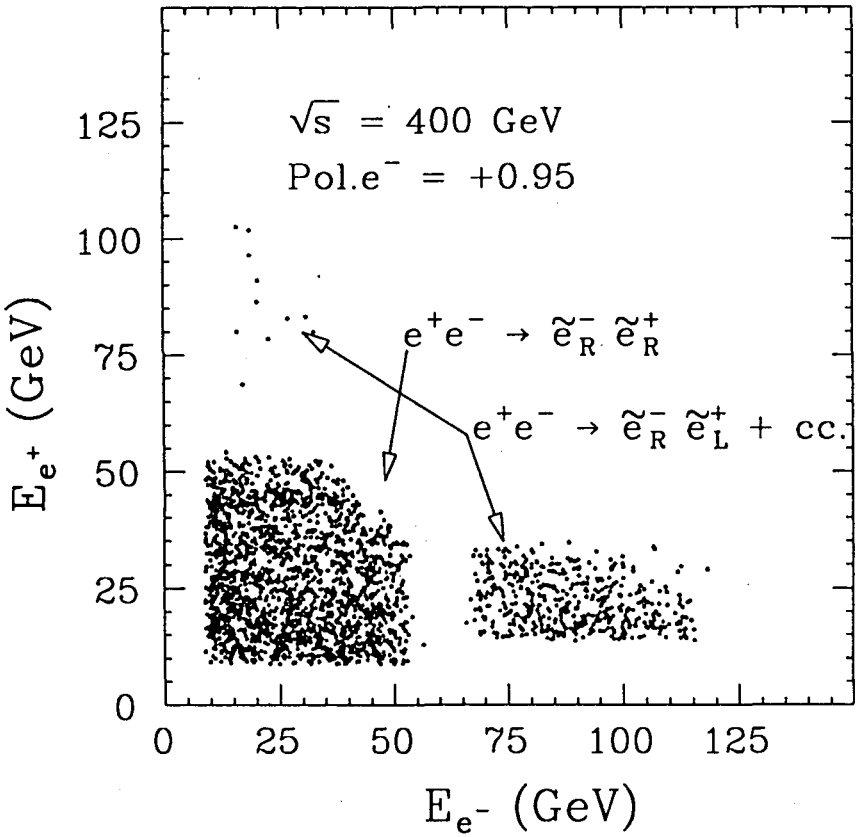
√s = 400 GeV
Pol.e⁻ = +0.95
e⁺e⁻ → ẽ⁻R ẽ⁺R
e⁺e⁻ → ẽ⁻R ẽ⁺L + cc.
E_e⁺ (GeV)
E_e⁻ (GeV)
0
25
50
75
100
125

Fig.17

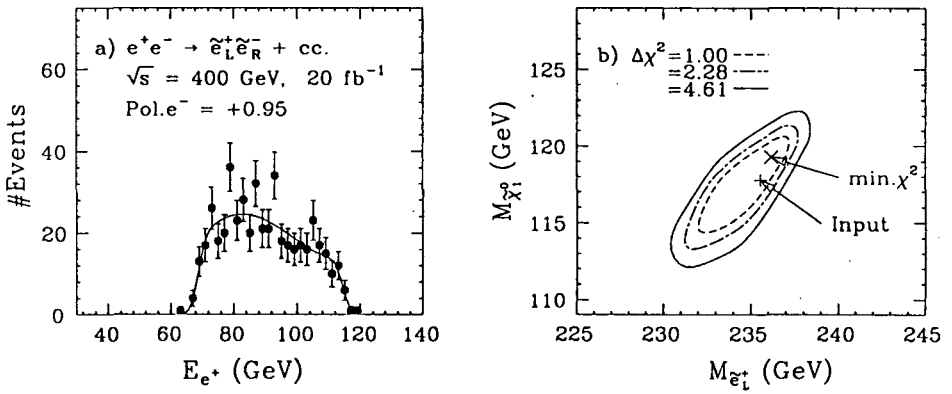
a) e⁺e⁻ → ẽ⁺Lẽ⁻R + cc.
√s = 400 GeV, 20 fb⁻¹
Pol.e⁻ = +0.95
#Events
E_e⁺ (GeV)
b) Δχ²=1.00
=2.28
=4.61
min.χ²
Input
M_χ̃⁰₁ (GeV)
M_ẽ⁺L (GeV)

Fig.18

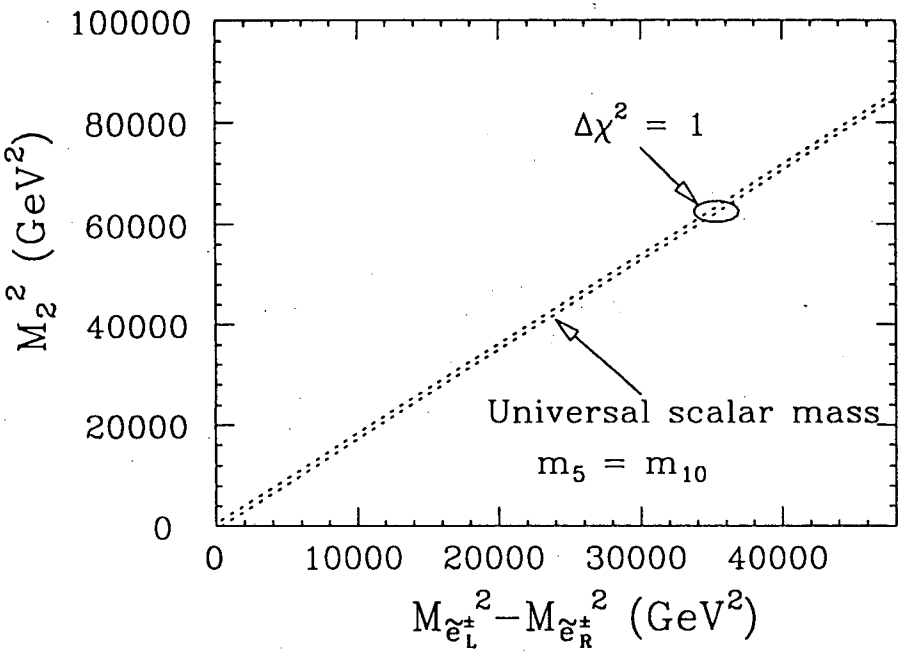
100000
80000
60000
40000
20000
0
M_2^2 (GeV^2)
$\Delta\chi^2 = 1$
Universal scalar mass
$m_5 = m_{10}$
0
10000
20000
30000
40000
$M_{\tilde{e}_L^\pm}^2 - M_{\tilde{e}_R^\pm}^2$ (GeV^2)

Fig.19

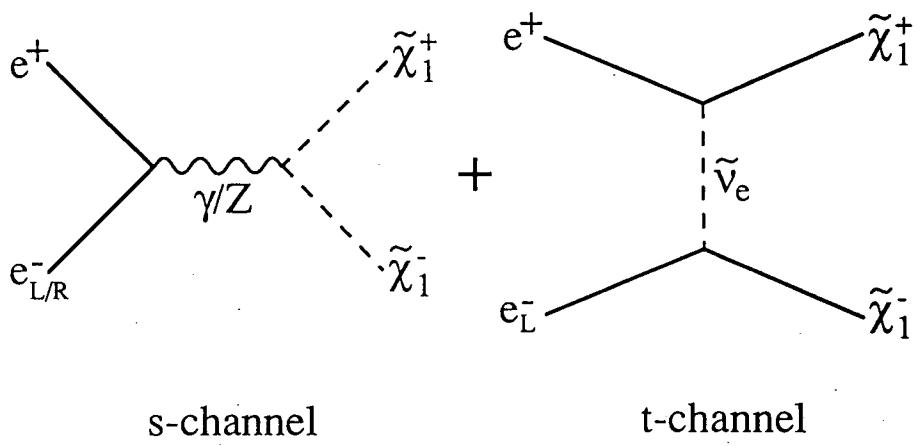
e^+
$e^-_{L/R}$
γ/Z
$\tilde{\chi}_1^+$
$\tilde{\chi}_1^-$
+
e^+
e^-_L
$\tilde{\nu}_e$
$\tilde{\chi}_1^+$
$\tilde{\chi}_1^-$
s-channel
t-channel

Fig.20

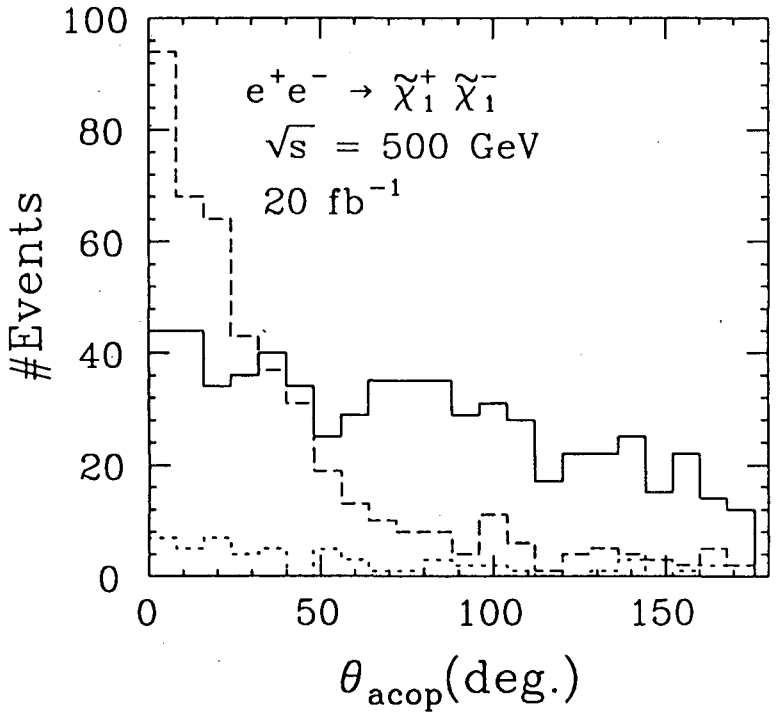
$e^+e^- \to \tilde{\chi}_1^+ \tilde{\chi}_1^-$
$\sqrt{s}$ = 500 GeV
20 fb^{-1}
#Events
θ_{acop}(deg.)

Fig.21

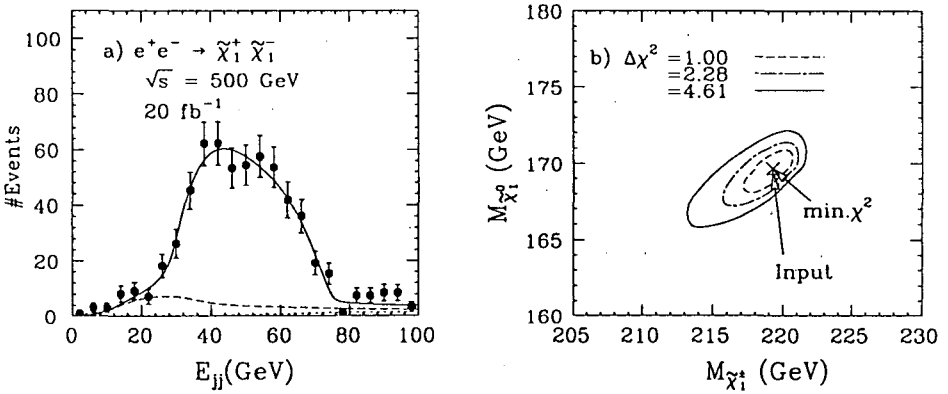
a) $e^+e^- \to \tilde{\chi}_1^+ \tilde{\chi}_1^-$
$\sqrt{s}$ = 500 GeV
20 fb^{-1}
#Events
E_{jj}(GeV)
b) $\Delta\chi^2$ =1.00
=2.28
=4.61
min.χ^2
Input
$M_{\tilde{\chi}_1^0}$ (GeV)
$M_{\tilde{\chi}_1^\pm}$ (GeV)

Fig.22